

To Be or not to Be: the role of rotation in modeling Galactic Be X-ray Binaries

KYLE AKIRA ROCHA,^{1,2} VICKY KALOGERA,^{1,2} ZOHEYR DOCTOR,^{2,1} JEFF J. ANDREWS,³ MENG SUN,² SETH GOSSAGE,²
SIMONE S. BAVERA,^{4,5} TASSOS FRAGOS,^{4,5} KONSTANTINOS KOVLAKAS,^{6,7} MATTHIAS U. KRUCKOW,^{4,5} DEVINA MISRA,^{4,8}
PHILIPP M. SRIVASTAVA,^{2,9} ZEPEI XING,^{4,5} AND EMMANOUIL ZAPARTAS^{10,11}

¹*Department of Physics & Astronomy, Northwestern University, 2145 Sheridan Road, Evanston, IL 60208, USA*

²*Center for Interdisciplinary Exploration and Research in Astrophysics (CIERA), 1800 Sherman, Evanston, IL 60201, USA*

³*Department of Physics, University of Florida, 2001 Museum Rd, Gainesville, FL 32611, USA*

⁴*Département d'Astronomie, Université de Genève, Chemin Pegasi 51, CH-1290 Versoix, Switzerland*

⁵*Gravitational Wave Science Center (GWSC), Université de Genève, CH1211 Geneva, Switzerland*

⁶*Institute of Space Sciences (ICE, CSIC), Campus UAB, Carrer de Magrans, 08193 Barcelona, Spain*

⁷*Institut d'Estudis Espacials de Catalunya (IEEC), Carrer Gran Capità, 08034 Barcelona, Spain*

⁸*Institutt for Fysikk, Norwegian University of Science and Technology, Trondheim, Norway*

⁹*Electrical and Computer Engineering, Northwestern University, 2145 Sheridan Road, Evanston, IL 60208, USA*

¹⁰*Institute of Astrophysics, FORTH, N. Plastira 100, Heraklion, 70013, Greece*

¹¹*IAASARS, National Observatory of Athens, Vas. Pavlou and I. Metaxa, Penteli, 15236, Greece*

ABSTRACT

Be X-ray binaries (Be-XRBs) are crucial in understanding high-mass X-ray binaries, featuring a rapidly rotating Be star and a neutron star companion in an eccentric orbit, intermittently accreting material from the Be star's decretion disk. Originating from binary stellar evolution, Be-XRBs are of significant interest to binary population synthesis (BPS) studies, encapsulating the physics of supernovae, common envelope, and mass transfer (MT). Using the POSYDON BPS code, employing pre-computed grids of detailed binary stellar evolution models, we investigate the Galactic Be-XRB population. POSYDON incorporates stellar rotation self-consistently during MT phases, enabling a detailed examination of the rotational distribution of Be stars. Our fiducial BPS and Be-XRB model align well with the orbital properties of Galactic Be-XRBs, emphasizing the role of rotational constraints. Our modeling reveals a bimodal rotational distribution of Be-XRB-like systems, in excellent agreement with literature values. All Be-XRBs undergo an MT phase before the first compact object forms, with over half experiencing a second MT phase from a stripped helium companion (Case BB). Computing rotationally-limited MT efficiencies and applying them to our population, we find that the majority of Be-XRBs have undergone highly non-conservative MT ($\beta_{\text{rot}} \simeq 0.15$). Our study underscores the importance of detailed angular momentum modeling during MT in interpreting Be-XRB populations, emphasizing this population as a key probe for the stability and efficiency of MT in interacting binaries.

Keywords: Astronomical simulations (1857); Multiple star evolution (2153); High mass X-ray binary stars (733); Be stars (142)

1. INTRODUCTION

Classical Be stars are understood to be rapidly rotating spectral-type B stars that have been observed with Balmer emission lines and excess infrared emission, attributed to a circumstellar, rotationally supported *decretion* disk emanating from the star (Rivinius et al.

2013). The idea that rapid rotation of Be stars is linked to the formation of the decretion disk, first proposed by Struve (1931), remains a leading theory for the so-called *Be-phenomenon*, as observations consistently show the Be population as a whole is highly spinning (e.g., Yudin 2001; Rivinius et al. 2013; Zorec et al. 2016; Balona & Ozuyar 2021; Kamann et al. 2023). Although the true rotational distribution of Be stars is in and of itself an active area of inquiry (e.g. Townsend et al. 2004; Yudin 2001; Rivinius et al. 2013; Balona & Ozuyar 2021;

Abdul-Masih 2023). While there have been extensive studies into the evolution of the disk in isolated Be stars and under the influence of a companion in a binary, the exact mechanism(s) responsible for launching the disk remain a topic of debate (Okazaki 1997; Okazaki et al. 2011; Martin et al. 2011, 2014; Panoglou et al. 2016; Cyr et al. 2017; Brown et al. 2018; Panoglou et al. 2018; Brown et al. 2019; Cyr et al. 2020; Franchini & Martin 2019, 2021; Suffak et al. 2022). Theories for decretion disk formation include non-radial stellar pulsations (Ressler 2021) and/or small scale surface magnetic fields (Nixon & Pringle 2020), but all require rapid rotation to effectively reduce the surface gravity at the stellar equator for material to be launched into a sustained decretion disk.

Yet another question is the origin of Be stars’ rapid rotation. One possibility is that Be stars are formed as isolated single stars. In this *single-star* path, Be stars may get their rotation from core contraction along the main sequence (MS) and/or simply have high birth spins, (e.g. Meynet & Maeder 2000; Mathew et al. 2008a; Hastings et al. 2021). Another possible scenario is that Be stars attain spin from binary (or higher order) interactions including binary mass transfer or stellar mergers (Kriz & Harmanec 1975; Pols et al. 1991; Dallas et al. 2022; Shao & Li 2014). The binary channel has recently gained favor due to a multitude of observations: Gaia space satellite measurements of the relatively lower binary fraction of Be vs. B field stars (Dodd et al. 2023); identification of Be star binaries with sub-dwarf (sdO, stripped helium star) companions (El-Badry & Quataert 2021; Ramachandran et al. 2023; Wang et al. 2023); and the discovery and characterization of Be stars with compact object (CO) companions, referred to as Be X-ray binaries (Be-XRBs; Reig 2011; Fortin et al. 2023).

In this work we model Be-XRBs, a subclass of high-mass X-ray binaries (HMXBs)¹ in which the CO accretes material from the decretion disk emanating from the central Be star, producing variable X-ray emission correlated with the H α emission from the disk (Okazaki 1997; Reig 2011). Nearly all Be-XRBs with characterized CO companions harbor neutron stars (NSs) (Reig 2011). There is one exception with a tentative BH Be-XRB claimed (MWC-656; Casares et al. 2014, however Janssens et al. 2023 favor a NS or lower mass companion). The general picture views Be-XRBs as the descendants of Be+sdO binaries which remain bound after the

sufficiently massive helium (He) star explodes in a supernova (SN). Be-XRBs have therefore garnered broad interest from binary stellar evolution studies as they encode the physics of supernovae (SNe), common envelope (CE), mass transfer (MT), etc. into their resulting observed populations (e.g. Pols et al. 1991; Belczynski & Ziolkowski 2009; Shao & Li 2014; Grudzinska et al. 2015; Vinciguerra et al. 2020; Xing & Li 2021; Misra et al. 2023; Liu et al. 2024, and others). The majority of the aforementioned studies use population-synthesis modeling techniques wherein single-star models (SSE, Hurley et al. 2000) and analytic prescriptions are combined to approximate the effects of MT on the star’s evolution, since computing self-consistent binary evolution sequences has hitherto been computationally infeasible. While the SSE formalism facilitates the generation of large scale populations, it cannot self-consistently model the angular momentum evolution of stars as they interact and evolve—a defining feature of Be stars in Be-XRBs.

To simultaneously model binary stellar evolution and mass transfer, we employ the next-generation BPS code POPulation SYNthesis with Detailed binary-evolution simuLatiONs (POSYDON). POSYDON relies on a new modeling paradigm, wherein binary stellar tracks computed with Modules for Experiments in Stellar Astrophysics (MESA; Paxton et al. 2011, 2015, 2013, 2018, 2019) are integrated within a BPS framework (Fragos et al. 2023). This novel treatment includes the self-consistent evolution (solving the equations of stellar structure and composition) of individual stellar spins accounting for tides, mass transfer, and spin-orbit coupling. We investigate the predicted rotational distribution of Be-XRB BPS models and compare our model Be-XRB population to the Galactic sample of observed Be-XRBs from Fortin et al. (2023).

In Section 2 we describe our data selection of Galactic Be-XRBs, and detail the relevant BPS modelling assumptions in POSYDON and our adopted Be-XRB selection criteria in Section 3. We compare our models to data in Section 4 and show how rotational modelling can naturally explain features of the observed Galactic Be-XRB population. Finally in Section 5 and Section 6 we discuss our findings and summarize with concluding remarks.

2. OBSERVED SAMPLE

For this study we use the newly updated catalog of 159 Galactic HMXBs compiled by Fortin et al. (2023). We select the subset of the catalog that includes systems with a firm Be-XRB classification and orbital solutions, excluding systems with tentative or hybrid classifica-

¹ The others being Supergiant XRBs (SGXB, Corbet 1986) and Supergiant Fast X-ray Transients (SFXTs, Negueruela et al. 2006) which primarily accrete through strong stellar winds from an evolved donor.

tions such as “Be?” or “Be/Sg”. We also exclude most gamma-ray binaries with Be companions since these systems may produce their high energy emission through interactions outside the canonical picture of a NS accreting from the decretion disk (e.g. white dwarf companions, magnetic field interactions, etc., [Langer et al. 2020](#)). Thus we include the systems which are seen to interact with the decretion disk of the donor (namely PSR B1259-63, [Hare et al. 2023](#)). We consider two subsamples of our selected Be-XRBs: *i*) all Be-XRBs with orbital period measurements, and *ii*) Be-XRBs with both orbital period and eccentricity measurements. Our resulting observed samples contain 46 and 18 systems respectively, listed in [Table 2](#).

This sample contains binaries with Be donor stars that are preferentially early B-type (B0–B2), span a range of orbital periods from 10-1000 days, and are generally eccentric. Their properties are listed in [Table 2](#).

3. METHODS

3.1. Population synthesis physics

To simulate a Galactic Be-XRB population, we use the POSYDON v1 ([Fragos et al. 2023](#)) binary population synthesis (BPS) code to evolve a population of two million binaries at solar metallicity with $Z = 0.0142$ and $Y = 0.2703$ ([Asplund et al. 2009](#)). In this section we provide a brief summary of our fiducial model parameters and key physical assumptions in our population synthesis.

To simulate a realistic population of interacting binaries, we draw their initial masses (M_1, M_2) and orbital periods (P_{orb}) using observationally motivated distributions. We draw primary masses using a Kroupa power law initial mass function (IMF, [Kroupa 2001](#)) with an index $\alpha = 2.3$, with a minimum mass of $7 M_{\odot}$ and maximum mass of $120 M_{\odot}$, corresponding to the limits of the detailed binary grids in POSYDON v1. Secondary masses are determined by sampling uniformly in the mass ratio $q = M_1/M_2$ in the bounds $[0, 1]$ ([Sana et al. 2013](#)) with a minimum allowed mass of $1 M_{\odot}$. Initial orbital periods are drawn following [Sana et al. \(2013\)](#) in the range $[1 \text{ day} - 10^{3.5} \text{ day}]$, and following a flat-in-log distribution from 1 day down to 0.35 day as described in [Fragos et al. \(2023\)](#). All binaries are initialized with circular orbits with stellar spins set to the orbital period, implying efficient tidal synchronization during the pre-main-sequence.

Binaries are evolved forward in time for 10 Gyr or until they end their life as a merger following an unsuccessful CE, a double CO merger, or a binary disruption). In the POSYDON framework, phases of binary evolution where Roche-lobe overflow (RLO) mass transfer can occur are

modeled using the results of detailed binary evolution simulations with MESA, where stars are evolved simultaneously with the orbit allowing self-consistent treatment of mass-transfer stability. We use initial-final linear interpolation and k -nearest neighbor classification in all binary grids as described by [Fragos et al. \(2023\)](#), to evolve a binary from an initial state through phases of evolution (e.g. RLO MT to SN, CE, etc.). To simulate SNe and CE phases, we utilize standard BPS prescriptions as described below.

Following POSYDON v1, systems enter dynamically-unstable RLO MT if the MT rate exceeds $0.1 M_{\odot} \text{ yr}^{-1}$, or if the stellar model expands beyond the outer Lagrange point L_2 , triggering the onset of common envelope evolution. We model CE using the $\alpha_{\text{CE}} - \lambda_{\text{CE}}$ formalism ([Webbink 1984](#); [Livio & Soker 1988](#)), where energy balance is used to determine if the envelope can be unbound with the orbital energy of the binary. The fraction of orbital energy released during the common envelope, α_{CE} , we set to 1, and the binding energy of the envelope, λ_{CE} , is calculated directly from profiles of our detailed MESA models using a core-envelope boundary defined by the mass shell where the central hydrogen (H) mass fraction drops below 10%. Systems that go through a successful CE with two H-rich stars are subsequently evolved as a detached system (i.e. two single stars).

We model SN explosions and compact object formation using the [Patton & Sukhbold \(2020\)](#) prescription for core-collapse SN (CCSNe), and the [Podsiadlowski et al. \(2004\)](#) prescription for electron-capture SN (ECSNe) for stars with final He core masses in the range of $1.4 - 2.5 M_{\odot}$. NSs receive natal kicks during the SN explosion which we draw from a Maxwellian distribution with a dispersion of $\sigma_{\text{CCSNe}} = 265 \text{ km s}^{-1}$ for CCSNe ([Hobbs et al. 2005](#)), and a dispersion of $\sigma_{\text{ECSNe}} = 20 \text{ km s}^{-1}$ for ECSN ([Giacobbo & Mapelli 2019](#)). The maximum mass of NSs is taken as $2.5 M_{\odot}$ ([Oppenheimer & Volkoff 1939](#)).

3.1.1. Rotationally-limited accretion in detailed binary models

POSYDON v1 binary models initialize two hydrogen-rich stars on the main sequence (HMS-HMS grid) in circular orbits, with stellar spins synchronized to the orbital period. We include self-consistent modeling of the angular momentum evolution of both stars including the effects of tides, spin-orbit coupling, mass-loss through stellar winds, and RLO mass-transfer ([Fragos et al. 2023](#)).

During HMS-HMS evolution we follow [Langer \(1998\)](#) and implement rotationally-limited accretion, assuming fully conservative RLO MT but including an enhanced stellar wind from the accretor (\dot{M}_{w}) which regulates the

stellar rotation below critical:

$$\dot{M}_w(\omega) = \dot{M}_w(0) \left(\frac{1}{1 - \omega/\omega_{\text{crit}}} \right)^{0.43}, \quad (1)$$

where ω is the equatorial surface rotation rate of the star, and $\omega_{\text{crit}}^2 = (1 - L/L_{\text{Edd}})GM/R^3$, where the exponent is taken from [Langer \(1998\)](#). We define the Eddington Luminosity as $L_{\text{Edd}} = 4\pi GMc/\kappa$, where we assume the opacity, κ , is dominated by Thompson scattering $\kappa = 0.2(1 + X) \text{ cm}^2 \text{ g}^{-1}$, where X is the hydrogen abundance of the star. Thus, the accretor may initially accept the mass transferred when its rotation is sub-critical, but at later times reject a significant amount of mass as the accretor approaches critical rotation, effectively halting further mass accretion.

3.1.2. Rotational Evolution in the detached phase

Binary systems may exit the two hydrogen rich stars (HMS-HMS) binary phase under multiple stopping criteria: the primary depleting central carbon (leading to a SN) or the binary undergoing unstable mass transfer (leading to CE). Systems which either remain bound after the first SNe, or survive a CE by successfully ejecting the envelope, will enter *detached evolution* of a star+CO.

We match the secondary stellar model at the end of the HMS-HMS simulations to an equivalent single-star model (matching criteria are evolutionary-phase dependant as described in [Fragos et al. 2023](#)) and continue evolving the orbit and stellar model until either RLO occurs or the stellar model reaches the end of its life. The rotation rate of the matched model is set such that they have an equivalent $\omega/\omega_{\text{crit}}$ as that of the secondary at the end of HMS-HMS evolution. The orbital evolution equations include tidal evolution with spin-orbit coupling and angular momentum loss from stellar winds. Our pre-computed single-star models are evolved without rotation and therefore cannot account for the back reaction onto the star’s structure and evolution.

3.2. Be-XRB modeling

For our study, we first select a *baseline* XRB candidate population: all systems which *i*) remain bound after the first SN, and *ii*) contain either a NS or black hole (BH). These systems will generally be eccentric with a stellar companion, and may exhibit detectable X-ray emission during their lifetime, depending on the orbital evolution and mass of the donor. It is this baseline XRB population that we use to extract subpopulations for comparisons to data.

Our modeling choices and selection criteria to categorize simulated binaries from the baseline population

as Be-XRBs are described in the following subsections: donor rotation (§3.2.1), donor mass (§3.2.2), disk interaction (§3.3.1), and X-ray luminosity (§3.3.2).

3.2.1. Stellar Rotation & the Be phenomenon

We adopt a conservative lower limit of $\omega/\omega_{\text{crit}} > 0.5$, above which donors are assumed to form a sustained decretion disk and appear as Be stars². While this lower limit on $\omega/\omega_{\text{crit}}$ is conservative compared to the higher values often adopted in BPS Be-XRB studies (e.g. [Misra et al. 2023](#); [Liu et al. 2024](#)), it is well within the range of recently reported measurements of the rotation rates of Be stars from as low as $\omega/\omega_{\text{crit}} = 0.3$, up to nearly critical values ([Frémat et al. 2005](#); [Cranmer 2005](#); [Zorec et al. 2016](#); [Balona & Ozuyar 2021](#)).

The diversity of measured rotation rates may be a consequence of the intrinsic efficiency of the Be phenomenon as a function of rotation ([Cranmer 2005](#)), evolutionary state ([Cochetti et al. 2020](#)), metallicity, etc. and or systematic biases from inferring rotation rates of rapidly rotating stars ([Townsend et al. 2004](#); [Frémat et al. 2005](#)). To explore this further, we also compare different regions of the rotational distribution within our threshold cutoff of $\omega/\omega_{\text{crit}} > 0.5$, to see if their origins can be interpreted through stellar and binary evolution processes.

3.2.2. Stellar mass

We chose a conservative mass cutoff for the donor star’s mass $M_d \gtrsim 3 M_\odot$, to investigate the role of rotation on the resulting Be-XRB subpopulation. While early O-type stars are not observed to exhibit the Be phenomenon, we refrain from imposing an upper mass limit in our definition of Be-XRBs as we seek to reproduce this feature self-consistently.

This lower limit on M_d aligns with other BPS Be-XRB studies which range from as low as $\simeq 3 M_\odot$ (e.g. [Xing & Li 2021](#); [Vinciguerra et al. 2020](#)) to be consistent with the spectral definition of B stars ([Harmanec 1988](#)), or as high as $\simeq 6 M_\odot$ (e.g. [Liu et al. 2024](#); [Misra et al. 2023](#)), based on masses most often reported in Be-XRB catalogues.

3.3. Accounting for observable lifetime

To compare our BPS models to the Galactic sample of Be-XRBs, we apply a constant star formation history to

² Whether the disk itself is observable depends upon the strength of H α emission and the duty cycle of the disk. For Galactic Be-XRBs, a negative H α equivalent width is the threshold for detection ([Reig 2011](#)), which, given our mass range and disk model, is achieved with modest disk sizes of 5-10 stellar radii ([Grundstrom & Gies 2006](#)), well within the radii of our adopted disk model.

our population at solar metallicity. We take 500 random, uniformly distributed time samples for the evolution of systems during their detached phase, where all samples for an individual system are weighted by the lifetime of the detached phase:

$$w_{t_{\text{det}}} = \frac{t_{\text{det}}}{t_{\text{H}}}, \quad (2)$$

where the detached phase lifetime, t_{det} , is defined as the time between the first SN and ends if RLO MT is initiated or if the stellar companion reaches the end of its life, and the normalization t_{H} is taken as the Hubble time. This weighting reflects the fact that longer-lived systems should appear more frequently for an impulsive, unbiased observation of the Galaxy. In total, from our initial population of 2 million binaries, our baseline CO+star population contains 1.5×10^8 unique evolutionary samples for the time evolving parameters of detached binaries.

3.3.1. Disk Interaction

To capture the transient X-ray emission of Be-XRBs, we adopt a decretion disk model to select systems which are in orbits close enough to interact and accrete material from the disk. We follow the formalism from Liu et al. (2024), assuming an isothermal temperature profile with $T = 0.6 T_{\text{eff,d}}$ (Carciofi & Bjorkman 2006), with the outer disk radius r_{disk} at the sonic point (Krtička et al. 2011):

$$r_{\text{sonic}} = 0.3 (v_{\text{Kep}}/c_s)^2 R_{\text{d}}, \quad (3)$$

where v_{Kep} is the equatorial Keplerian orbital velocity $v_{\text{Kep}} = \sqrt{GM_{\text{d}}/R_{\text{d}}}$, c_s is the sound speed $c_s = \sqrt{2k_{\text{B}}T_{\text{eff,d}}/m_{\text{p}}}$, where k_{B} is Boltzmann's constant and m_{p} is the proton mass. Beyond the sonic point, the Keplerian orbital velocity in the disk is subsonic, leading to weak viscous coupling.

As there exists a diversity of choices among disk models between BPS studies, we also consider a simpler treatment implemented by Misra et al. (2023), where the maximum disk radius is taken as $100 R_{\text{d}}$, motivated by measurements of Be disk radii ranging from $30 - 150 R_{\text{d}}$ (Klement et al. 2017). We compare both models further in §4.2.

We define binaries which have periapse distances, $r_{\text{peri}} = a(1 - e)$ where a is the orbital semi-major axis, less than the disk radius, $r_{\text{peri}} < r_{\text{disk}}$, as interacting sources, where the X-ray luminosity is calculated in §3.3.2. We assume the disk has a constant radius as long as the donor is above the threshold rotation rate for the Be phenomenon to occur.

3.3.2. X-ray Luminosity

To simulate the X-ray luminosity of the Be-XRBs in our sample and determine whether a given system is observable, we adopt the formalism presented by Liu et al. (2024). The X-ray luminosity is calculated by first deriving a scaling relation between the mass accretion rate onto the CO (\dot{M}_{CO}) as a function of the periastron separation (r_{peri}) and base gas surface density (Σ_0) of the disk, $\dot{M}_{\text{CO}} \propto r_{\text{peri}}^{-2} \Sigma_0$, using the smoothed-particle hydrodynamics (SPH) simulations by Brown et al. (2019). Then Liu et al. (2024) normalize the accretion rate by deriving another scaling relation between decretion disk surface densities and the mass of the donor star (M_{d}), $\Sigma_0 \propto M_{\text{d}}^{1.44}$, using observations of Milky Way Be star disks from Vieira et al. (2017). Finally they adjust correction factors accounting for uncertainties in the SPH simulations and conversion between bolometric and X-ray luminosity, to best match their synthetic population to the empirically-derived peak X-ray luminosity function from Raguzova & Popov (2005):

$$\log(L_{\text{X}}/[10^{35} \text{ erg s}^{-1}]) = 4.53 \pm 0.66 - (1.50 \pm 0.33) \log(P_{\text{orb}}/\text{day}). \quad (4)$$

The final equations for calculating the X-ray luminosity for our binaries are as follows:

$$L_{\text{bol}} = \epsilon \dot{M}_{\text{CO}} c^2 = f_{\text{corr}} \times 5 \times 10^{36} \text{ erg s}^{-1} \times \left(\frac{\epsilon}{0.2}\right) \left[\frac{(1-e)a}{100 R_{\odot}}\right]^{-2} \left(\frac{\Sigma_0}{0.015 \text{ g cm}^{-2}}\right) \left(\frac{M_{\text{CO}}}{1.4 M_{\odot}}\right)^2 \quad (5)$$

where $f_{\text{corr}} = 0.5$ is the correction factor between the bolometric and X-ray luminosity, $\epsilon = 0.2$ is the efficiency of converting gravitational potential energy to radiation, M_{CO} is the compact object mass, and Σ_0 is the base gas density of the donor star's decretion disk:

$$\log(\Sigma_0/[g \text{ cm}^{-2}]) = 1.44 \log(M_*/M_{\odot}) - 2.37 + \mathcal{N}(0, 0.52), \quad (6)$$

where M_* is the mass of the donor star and $\mathcal{N}(0, 0.52)$ is a normal distribution with zero mean and standard deviation of 0.52, encapsulating the intrinsic scatter seen in the observed distribution of Be disk surface densities (Vieira et al. 2017). For a detailed derivation of Equation 5 and Equation 6, see Liu et al. (2024).

To model the detection of high energy emission of Galactic Be-XRBs, we use a threshold X-ray luminosity of $L_{\text{X}} = 10^{34} \text{ erg s}^{-1}$ above which binaries are considered detectable. This limit is motivated by the distribution of X-ray luminosities for Be-XRBs observed in the Milky Way (Brown et al. 2018).

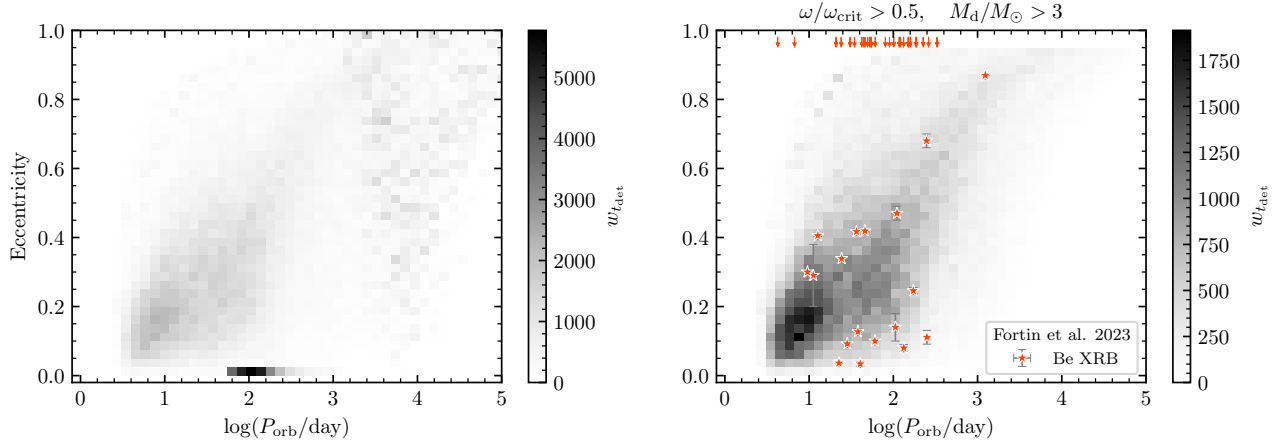


Figure 1. Two-dimensional histogram of the time-sampled orbital properties of our binary population, weighted by their detached lifetime $w_{t_{\text{det}}}$. The left panel shows the baseline population (a non-degenerate star with a CO companion) of candidate XRBs while the right panel shows our model Be-XRB subpopulation with our selected sample of Galactic Be-XRBs (from Fortin et al. (2023), listed in Table 2) is overlaid for comparison. Orange stars and arrows indicate observed Be-XRBs with $P_{\text{orb}} - e$ and only P_{orb} measurements, respectively.

4. RESULTS

4.1. Comparison to observed systems

To consider the accuracy of our Be-XRB modeling, we compare to observed distributions of systems in the plane of P_{orb} and eccentricity e shown in Figure 1, where all detached systems’ time-sampled evolution is weighted by their detached lifetime as in Equation 2. The left panel shows the baseline population containing CO+star binaries, with three main groups: an excess of circular systems at $\log(P_{\text{orb}}/\text{d}) \simeq 2$, moderately eccentric binaries at $\log(P_{\text{orb}}/\text{d}) \simeq 0.5 - 2.5$, and higher eccentricity, wide systems with $\log(P_{\text{orb}}/\text{d}) \gtrsim 3$. The right panel shows the Be-XRB subpopulation after applying our modeling selection criteria onto the baseline population, with observed Be-XRBs from Fortin et al. (2023) overlaid (systems listed in Table 2). Our selection criteria for Be-XRBs (§3.2), are systems which simultaneously satisfy the following: rapid donor rotation ($\omega/\omega_{\text{crit}} > 0.5$), B-type donor mass ($M_d > 3 M_\odot$), interaction with the decretion disk ($r_{\text{peri}} < r_{\text{disk}}$), and X-ray bright ($L_X > 10^{34} \text{ erg s}^{-1}$). As an initial comparison, our fiducial modeling can reproduce the broad orbital characteristics of Galactic Be-XRBs, with a high density of our models in the short period $\log(P_{\text{orb}}/\text{d}) \simeq 1$, low eccentricity $e \lesssim 0.2$ region, which we discuss further in 5.1. Furthermore, our simulated population exhibits a similar correlation between orbital period and eccentricity to that in the observed population.

We also compare the one-dimensional $\log_{10}(P_{\text{orb}}/\text{d})$ distribution between our baseline and Be-XRB model populations in Figure 2 with the observed period distribution with 46 systems listed in Table 2. Our mod-

els have a slight preference towards shorter orbital periods, with a flat peak around $\log(P_{\text{orb}}/\text{d}) \simeq 1 - 2$, compared to the observed population which appears to be peaking closer to $\log(P_{\text{orb}}/\text{d}) \simeq 2$. Overall, the majority of the orbital period distribution of our Be-XRB models and the observed population overlap with minima and maxima around $\log_{10}(P_{\text{orb}}/\text{d}) \simeq 0.5$ and $\log_{10}(P_{\text{orb}}/\text{d}) \simeq 3.5$, respectively.

We show in Figure 3 the simulated peak X-ray luminosities for our Be-XRB models before applying our X-ray luminosity threshold cutoff ($10^{34} \text{ erg s}^{-1}$ in §3.3.2), weighted by their detached lifetime. We recover the empirical relation of Raguzova & Popov (2005) in Equation 4 showing a correlation between the orbital period and peak X-ray luminosity of Be-XRBs, where the bulk of our models are well above our chosen luminosity threshold. Similar to Liu et al. (2024), we find a small population of ultra-luminous X-ray sources (ULXs) with $L_X > 10^{39} \text{ erg s}^{-1}$ and $\log(P_{\text{orb}}/\text{d}) \simeq 1$, which are faint in the figure due to their relatively rarity and shorter lifetimes.

4.2. Effect of the Decretion Disk Model

We find that the choice of decretion disk model as described in §3.3.1 has a negligible effect on the simulated Be-XRB population. In both disk models, we find that the majority of our binary models satisfy our disk interaction criteria, $r_{\text{peri}} < r_{\text{disk}}$. Comparing the two maximum disk radii together for all donors we find 97% of systems have $r_{\text{sonic}} > 100 R_d$. When applying the disk models within the orbital configurations of our baseline population, we find 97% and 86% of systems satisfy our interaction criterion using r_{sonic} and $100 R_d$

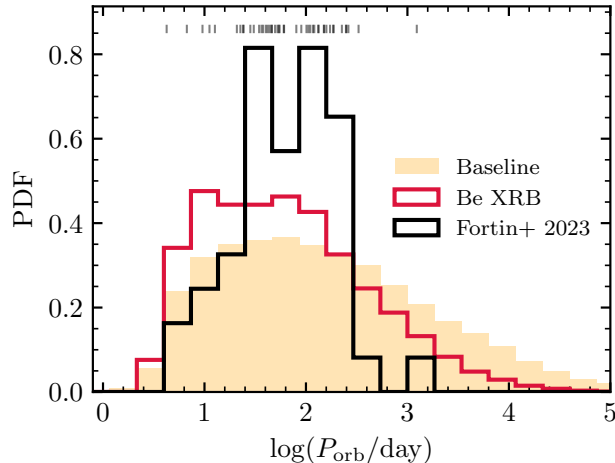


Figure 2. One-dimensional distributions of $\log_{10}(P_{\text{orb}}/\text{d})$ for our baseline (tan) and Be-XRB population (red) weighted by their detached lifetime ($w_{t_{\text{det}}}$), compared to the observed period distribution (black) compiled from Fortin et al. (2023). The small bars at the top of the plot indicate the individual systems within the histogram.

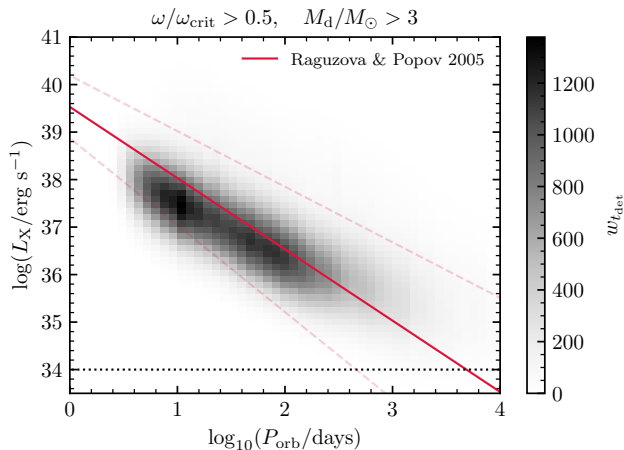


Figure 3. Predicted X-ray luminosity as a function of P_{orb} for our Be-XRB population weighted by their detached lifetime ($w_{t_{\text{det}}}$). The red lines show the mean (solid) and uncertainty (dashed) from the empirical relation from Raguzova & Popov (2005) provided in Equation 4. The black dotted line shows our chosen threshold X-ray luminosity.

respectively. Furthermore, Figure 10 shows negligible differences in the rotation rates, masses, orbital parameters, and luminosities of Be-XRBs between the two disk models, suggesting the disk interaction criterion is not the leading uncertainty in the present study.

4.3. Effect of the Rotation and Mass Cuts

To interpret the physical effects of our Be-XRB selection criteria, we compare the critical rotation and

donor mass constraints individually in Figure 4, showing one-dimensional parameter distributions weighted by a system’s detached lifetime from Equation 2. This serves as an approximate comparison between traditional BPS selection criteria identifying Be-XRB donors using only mass cuts, and our criteria with POSYDON which also rely upon self-consistent modeling of the rotation and accretion during the prior RLO MT phase. The gray distribution shows the baseline population of CO+star binaries, while the solid green and dashed pink distributions show systems containing rapidly rotating donors with $\omega/\omega_{\text{crit}} > 0.5$ or massive B-type donors with $M_d > 3 M_{\odot}$, respectively.

Using a rotation criterion of $\omega/\omega_{\text{crit}} > 0.5$ selects binary systems with donor masses in the range $\sim 2 - 25 M_{\odot}$, more NS companions than BHs, and non-circular binaries peaking with $e \simeq 0.25$ and orbital periods around $\log_{10}(P_{\text{orb}}/\text{d}) \sim 1 - 2$ with a tail falling off at wider orbital periods. Cutting only on donor mass spans a wide range of rotation rates extending below our fiducial cut of $\omega/\omega_{\text{crit}} > 0.5$, and including a large fraction of the highly spinning systems. This cut also contains binaries with more BHs and selects a large fraction of circular systems.

The subpopulation identified as Be-XRBs using the critical rotation criterion alone is in better agreement with observations than using donor mass alone, which we discuss further in §5.2.

4.4. Characteristic Evolution of Be-XRBs

It has long been suggested that Be-XRBs primarily form through the stable mass-transfer channel, wherein the initially more massive star spins up the secondary through MT while on the MS, before subsequently experiencing core-collapse and leaving behind a compact object with a Be companion in a Be-XRB (Rappaport & van den Heuvel 1982; Pols et al. 1991; de Mink et al. 2013). In this work we confirm this standard formation scenario, finding that the vast majority of systems we categorize as Be-XRBs have gone through stable mass transfer while on the MS ($\gtrsim 99\%$). A much smaller fraction of systems have not gone through any RLO MT, and a negligible fraction ($\lesssim 0.01\%$) are forming through a common envelope. While more binaries in our initial population generally survive common envelope, they often do not become Be-XRBs as the surviving helium cores are not massive enough ($\lesssim 2.5 M_{\odot}$) to undergo a SN, forming a CO.

Branching fractions for the baseline and Be-XRB populations are presented in Table 1, categorized by a system’s mass-transfer history during their MS evolution. To summarize the details of a system’s evolution which

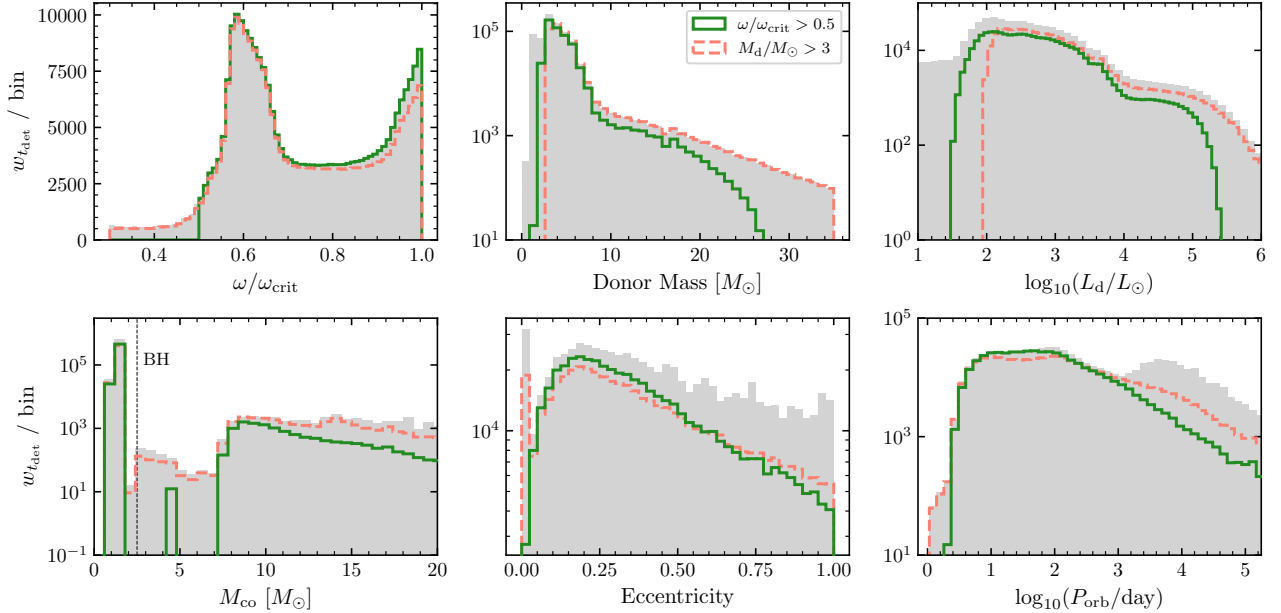


Figure 4. One-dimensional parameter histograms of the baseline population (gray), compared to cuts on rotation (solid green) or donor mass (dashed pink) alone. During the detached phase, we randomly sampled uniformly each binary’s time evolution and weight samples by the lifetime of the binary ($w_{t_{\text{det}}}$ defined in Equation 2). While we combine multiple selection criteria simultaneously to determine Be-XRBs in our population synthesis, we use these individual cuts to demonstrate the physical importance of each cut when constraining our Be-XRB population with rotational modeling ($\omega/\omega_{\text{crit}} > 0.5$).

may involve multiple phases of RLO MT, we use standard definitions of MT phases: Case A, Case B, and Case C, where each letter corresponds to MT during the MS, Hertzsprung-gap (or stripped He star), or an evolved state, respectively (Iben 1991). Systems which undergo successive phases of MT are denoted with multiple letters separated by slashes (e.g. we denote Case A followed by Case B as Case A/B) as introduced by Fragos et al. (2023).

In the baseline population of CO+star binaries, the largest number of systems go through Case B (34%), Case B/C/BB MT (20%), or have no RLO MT on the MS (15%). Case B/C/BB MT describes stars which initiate MT after reaching Terminal Age Main Sequence (TAMS) continuing into the star’s giant phase, followed by another phase of MT from the now stripped He star as it leaves the He MS. While Case B and Case B/C/BB systems have a high probability of evolving into Be-XRBs (56% and 87% respectively), systems which do not enter RLO have a low probability (2%) of becoming Be-XRBs, making up $\lesssim 0.1\%$ of the entire weighted Be-XRB population. We find almost half our weighted Be-XRB population (47%) have gone through Case B/C/BB evolution, with the remaining majority going through Case B (20%), Case B/BB (15%), or Case B/C (14%). In total, $\simeq 64\%$ of the weighted Be-XRBs have gone through a phase of Case BB MT, while those

systems only going through Case A or Case A/B contribute $\simeq 1.5\%$.

To further investigate the physical processes leading to the Be-XRB phase identified from Section 4.3, we show in Figure 5 the time-series evolution of one such system taken at random from our population synthesis models. This binary goes through Case B MT initiated by the primary with an initial mass of $\sim 7.5 M_\odot$, where about $5 M_\odot$ of material is transferred through RLO to the secondary star, leaving behind the $\sim 2.5 M_\odot$ He core. During MT, the secondary quickly reaches critical rotation from the mass accretion (Packet 1981), causing the majority of the subsequent mass transferred from the primary to be lost through the rotationally-enhanced winds of the accretor (Equation 1 described in 3.1.1). As a result of the mass and angular momentum loss from the system, the binary widens, increasing the orbital period which stabilizes the system as it naturally exits the MT phase into a detached binary containing a He and H-rich star. Then ~ 3 Myr after MT, the primary, which is now a stripped He star, undergoes a SN forming a NS in an $e \simeq 0.18$, 30 day orbit with a $7.4 M_\odot$ rapidly rotating companion.

This marks the beginning of this binary’s Be-XRB phase, where the secondary has evolved $\simeq 20\%$ of its MS lifetime. As the secondary continues on the MS, its radius expands, causing a steady increase in $\omega/\omega_{\text{crit}}$ until it reaches TAMS. While the eccentricity remains

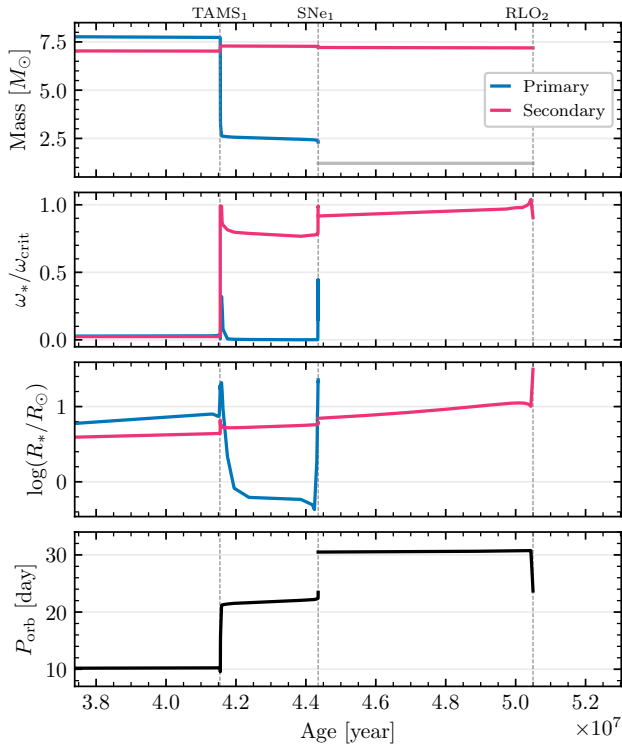


Figure 5. Characteristic time-series evolution of a Be-XRB from our population evolving from ZAMS, through Case B MT until the first SN, and into the detached phase. The discontinuity after SNe₁ (e.g. total mass and radius) is from two effects: *i*) the detailed binary model used for HMS-HMS evolution is the nearest neighbor track (while IF interpolation was used to evolve the population), and *ii*) the matching criteria taking the secondary star post HMS-HMS evolution mapping to an equivalent non-rotating single star model. This binary ends up merging during common envelope evolution after MT is initiated by the secondary. The majority of Be-XRBs in our population eventually end through mergers since their mass ratio is extreme and are therefore more likely to enter dynamically unstable MT.

nearly unchanged during the detached phase, there is a short period when the eccentricity increases as the stellar spin angular momentum is redistributed by tides into the orbit. If the spin angular momentum of the star is comparable to the orbital angular momentum, this can lead to eccentricity increases of nearly $e \simeq 0.1$ in the most extreme cases, and in general extends the lifetime of binaries in their eccentric configuration.

Since our present study is focused on the role of rotation in Be-XRB modeling, we show in Figure 6 the evolution of the rotational distribution of secondary stars at multiple evolutionary phases: at ZAMS, the moment before the first SNe (post MT), and a time sampled distribution during the detached phase, weighted by $w_{t_{\text{det}}}$ from Equation 2. The dashed lines tracing the Be-XRB

subpopulation, show that all systems have relatively low rotation rates at ZAMS with $\omega/\omega_{\text{crit}} \lesssim 0.2$, and are spun up through RLO MT. Prior to the first SN, the rotational distribution has shifted closer to critical with the majority of systems having $\omega/\omega_{\text{crit}} \gtrsim 0.5$. Then, as systems evolve during the detached phase, depending on their orbital and donor properties, tides serve to synchronize the rotation rate with the orbital period, effectively slowing down the donor stars, causing the peak of the distribution to shift to lower values at $\omega/\omega_{\text{crit}} \simeq 0.6$. Also present in the detached rotational distribution is a secondary peak at $\omega/\omega_{\text{crit}} \simeq 0.99$, caused by a star’s gradual expansion as it approaches TAMS, decreasing w_{crit} (Meynet & Maeder 2000; Hastings et al. 2021). We also note the large bifurcation between slowly rotating ($\omega/\omega_{\text{crit}} \simeq 0$) and moderate to rapidly rotating systems ($\omega/\omega_{\text{crit}} \gtrsim 0.5$), due to the strong dependence of tidal evolution on the separation of the binary and radius of the star (Hut 1981).

As a result of MT during the HMS-HMS evolution, secondaries are spun up to a wide distribution of rotation rates before entering their detached evolutionary phase with peaks at $\omega/\omega_{\text{crit}} \simeq 0$, $\omega/\omega_{\text{crit}} \simeq 0.75$, and $\omega/\omega_{\text{crit}} \simeq 0.99$.

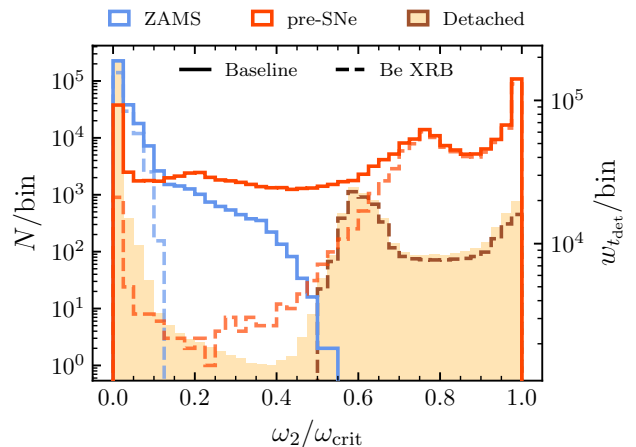


Figure 6. Rotational evolution of our baseline and Be-XRB population at different phases of stellar evolution: at ZAMS, pre-SN, and the subsequent time sampled evolution during the detached XRB phase, weighted by the system’s lifetime ($w_{t_{\text{det}}}$). Both ZAMS and pre-SN distributions contain instantaneous values for an individual system. The solid lines show the baseline population comprised of CO+star binaries, while the dashed lines show the Be-XRB population. The transformation between the ZAMS rotational distribution at relatively low values of $\omega/\omega_{\text{crit}}$, and the pre-SN distribution is a direct result of the angular momentum gained through RLO MT during their HMS-HMS evolution.

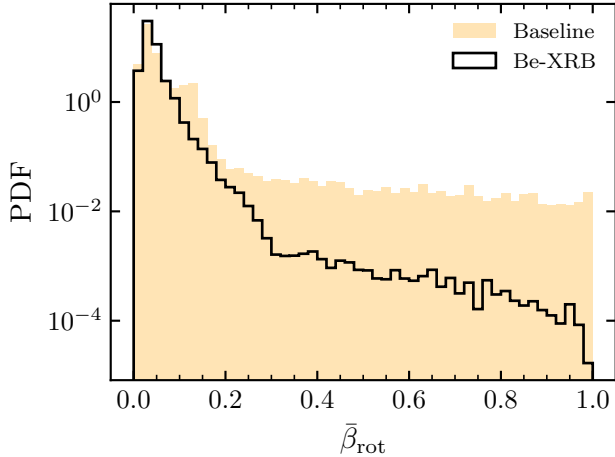


Figure 7. Rotationally-limited mass-transfer efficiency ($\bar{\beta}_{\text{rot}}$ as in Equation 8) of our population synthesis models evolving through their HMS-HMS evolution, weighted by their detached lifetime $w_{t_{\text{det}}}$. In our binary models, the accretor can reject significant amounts of the matter transferred during RLO MT via its enhanced wind (as a function $\omega/\omega_{\text{crit}}$), which keeps the star rotating below critical.

4.5. Mass Transfer Efficiency

A commonly explored parameter in BPS studies is the mass-transfer efficiency, $\beta \equiv \Delta M_{\text{acc}}/\Delta M_{\text{donor}}$, determining how much mass transferred through RLO is successfully accreted by the donor (Hurley et al. 2002). In order to compare our rotationally-limited accretion models described in §3.1.1 to the standard population synthesis MT efficiency β , we calculate an effective rotationally-limited MT efficiency metric:

$$\beta_{\text{rot}} = \frac{\Delta M_{\text{acc}}}{\Delta M_{\text{d,RLO}}}, \quad (7)$$

where ΔM_{acc} is the mass gained by the accretor, and $\Delta M_{\text{d,RLO}}$ is mass lost from the donor through a phase of Roche-lobe overflow MT (defined as the sequences when the mass-transfer rate exceeds a threshold value: $\dot{M}_{\text{RLO}} > 10^{-15} M_{\odot} \text{ yr}^{-1}$). Our models often contain multiple discrete phases of MT (e.g. case A/B/BB), which would produce multiple values for β_{rot} for an individual simulation. Therefore, for this initial comparison, we perform a mass-weighted average of simulations with n total MT phases:

$$\bar{\beta}_{\text{rot}} = \frac{1}{M_{\text{tot}}} \sum_{i=1}^n \beta_{\text{rot},i} \cdot \Delta M_{\text{acc},i}, \quad (8)$$

where i indexes individual phases of MT, the mass weight $\Delta M_{\text{acc},i}$ is the mass gained by the accretor during the i 'th phase, and $M_{\text{tot}} = \sum \Delta M_{\text{acc},i}$ is the total mass gained by the accretor through the simulation.

This rotationally-limited MT efficiency $\bar{\beta}_{\text{rot}}$ is then calculated for every model in our HMS-HMS grid and included in the same Initial-Final interpolation scheme used to evolve our binary population as described in Fragos et al. (2023), which is then applied on our astrophysical binary population shown in Figure 7.

The baseline and Be-XRB populations have a strong peak at $\bar{\beta}_{\text{rot}} \simeq 0.05$ with a long tail to higher MT efficiencies. The Be-XRB population is less likely to evolve through more conservative RLO MT ($\bar{\beta}_{\text{rot}} \gtrsim 0.2$) because *i*) they are intrinsically rare in the baseline as they are near regions of dynamically unstable MT, and *ii*) the accretors are not spun up to large values of $\omega/\omega_{\text{crit}}$, and are therefore short lived in their Be phase.

4.6. Changing the critical rotation threshold for the Be phenomenon

In Figure 8, we investigate the differences between simulated systems which population different peaks in the simulated rotational distribution. We show one-dimensional weighted distributions of our population during their detached phase, selecting systems with intermediate rotation at $\omega/\omega_{\text{crit}} \simeq 0.6$ and systems with nearly critical rotational $\omega/\omega_{\text{crit}} \simeq 0.99$. Similar to the analysis in Figure 4, we find the peaks in the bimodal rotational distribution are well separated in other binary and stellar parameters. For the intermediate rotation population, we see that donors can be as massive as $\sim 30 M_{\odot}$, systems contain more BHs as CO companions, with a nearly flat eccentricity distribution, and an orbital period distribution peaking closer to 100 days. In contrast the critically rotating population contains donors with masses only up to $\sim 10 M_{\odot}$, fewer BH companions, a skewed eccentricity distribution peaking around 0.2, and an orbital period distribution peaking closer to 10 days.

We also vary our choice of threshold rotation ($\omega/\omega_{\text{crit}} > 0.5$ in our fiducial model), above which we assume the Be phenomenon is fully efficient. In Figure 9 we show the impact of this choice on a summary statistic: the weighted number ratio of BH to NS Be-XRBs ($W_{\text{BH}}/W_{\text{NS}}$, where $W_{\text{CO}} = \sum w_{t_{\text{det,CO}}}$) as a function of the critical rotation cut, as this ratio is sensitive to the physical channels producing Be-XRBs (Belczynski & Ziolkowski 2009).

Initially, the ratio of BH to NS Be-XRBs is around ~ 0.3 with no rotation constraints and monotonically decreases down to about 10^{-4} at $\omega/\omega_{\text{crit}} \simeq 0.95$. After an initial plateau, there is a sharp decrease around $\omega/\omega_{\text{crit}} \simeq 0.5$, after which $W_{\text{BH}}/W_{\text{NS}}$ drops by 2 orders of magnitude.

5. DISCUSSION

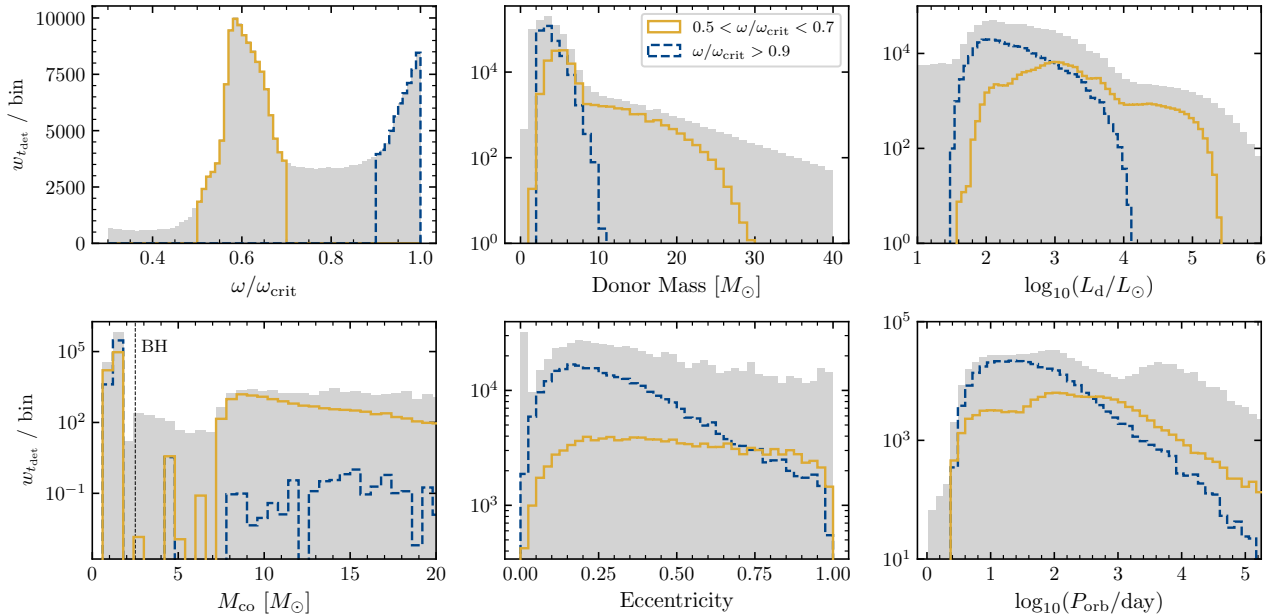


Figure 8. One-dimensional distributions of our time-sampled detached binary population (weighted by their detached lifetime $w_{t_{\text{det}}}$), showing the intermediate ($\omega/\omega_{\text{crit}} \simeq 0.6$, solid yellow) and critical ($\omega/\omega_{\text{crit}} \simeq 0.99$, dashed blue) rotation peaks in donor and CO mass, and orbital properties. Overall the two rotational peaks are well separated in donor mass and luminosity, CO mass, and binary orbital properties.

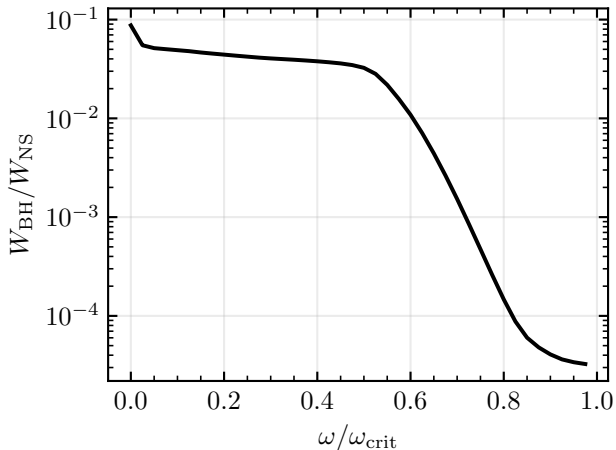


Figure 9. Weighted fraction of BH to NS Be-XRBs in our population as a function of the critical rotation $\omega/\omega_{\text{crit}}$, above which we assume the Be phenomenon is efficiently produced.

5.1. Matching with Galactic Be-XRBs

Our fiducial BPS modeling and Be-XRB selection criteria show good agreement with the orbital properties and X-ray luminosities of the observed sample of Galactic Be-XRBs. However, there are some notable discrepancies between our fiducial model and the observed data: We predict more systems with both low eccentricity and low orbital periods than in the observed sample. This apparent overprediction of systems at short orbital peri-

ods is seen in other BPS studies as well, within the range of commonly explored parameters (e.g. RLO MT efficiency or SN model Shao & Li 2014; Vinciguerra et al. 2020). Furthermore, tidal truncation of the decretion disk may explain the paucity of short-period Be-XRBs, with an estimated minimum at $P_{\text{orb}} \simeq 3$ days (Panoglou et al. 2018), which is in good agreement with our models as seen in Figure 2. Future studies with POSYDON may explore the contribution between selection effects and binary evolution physics in forming the short-period Be-XRB population.

5.1.1. On selection effects

In this work, we only perform qualitative comparisons to the observed Galactic Be-XRB population because we do not account for all observational selection effects, which could induce apparent differences between the observed and predicted system parameters. Notably, in Figure 1, some orbital configurations which have support in our model do not have corresponding observed systems with full orbital solutions. Importantly, though, our fiducial model does produce some support for the values of all observed Be-XRB systems, including the nearly circular systems at $P_{\text{orb}} \simeq 100$ days. Future investigations may implement more complete selection effects, though we note that these effects are complex: X-ray activity duty cycles (folding in decretion disk growth/dissipation (Vieira et al. 2017) and details of accretion efficiency (Brown et al. 2018)), donor character-

ization (dependent on luminosity estimates and associations/field crowding; Laycock et al. 2010), and successful eccentricity measurement. With a full understanding of the selection effects of our Be-XRB catalog, a comprehensive parameter study comparing observations with our models from POSYDON may also be performed.

5.2. Comparison of Be-XRB selection criteria: rotation and donor mass

A key finding of our simulations is that the critical rotation criterion ($\omega/\omega_{\text{crit}} > 0.5$) is primarily responsible for matching a majority of features in the observed Be-XRB population. Rotation naturally selects binaries with donor masses in the range $\sim 3 - 25 M_{\odot}$, which is within the canonical B to late O-type mass range (Harmanec 1988). Donor stars with $M_d \lesssim 2 M_{\odot}$ are excluded due to magnetic braking efficiently spinning them down, while massive O stars with $M_d \gtrsim 25 - 30 M_{\odot}$ are excluded due to their higher wind mass-loss rates, efficiently removing spin angular momentum from the star. This is consistent with effects observed in studies focusing on the emergence of the Be phenomenon in single stars (Meynet & Maeder 2000; Hastings et al. 2021).

In terms of orbital properties, high rotation selects systems which are preferentially eccentric, as systems which are initially eccentric from the SN and circularize from tides necessarily have the stellar spin synchronized ($\tau_{\text{synch}} < \tau_{\text{circ}}$, Hut 1981; Burkart et al. 2012), and for the standard Be donors observed in Be-XRBs, their synchronized rotation rates are well sub-critical³. This is consistent with the subset of Be-XRBs with complete orbital solutions, showing a preference for non-circular binaries (Fortin et al. 2023). While the majority of observed Be-XRBs have orbital periods $\gtrsim 10$ days, we see that rotational evolution alone is not sufficient to match this lower limit. This may be due to enhanced gravitational truncation effects that limit the formation of the decretion disk at short orbital periods (Okazaki et al. 2002; Panoglou et al. 2018).

Finally in the CO mass distribution, rapid rotation selects a majority of systems containing NSs relative to BHs, consistent with the observed sample being almost entire NS thus far (Reig 2011), and previous theoretical studies explaining the missing BH Be-XRB problem (Belczynski & Ziolkowski 2009). We find this is primarily driven by the relative rarity of BH progenitor stars and their prior evolution during the HMS-HMS phase.

³ For example, a tidally synchronized star of $15 M_{\odot}$ with radius $20 R_{\odot}$ in a 5 day orbit has a rotation rate of only $\omega/\omega_{\text{crit}} \simeq 0.1$, well outside the range for observed Be stars (Cranmer 2005; Zorec et al. 2016; Balona & Ozuyar 2021).

5.3. Mass-transfer history

Overall, our BPS models are in agreement with the standard formation scenario for Be-XRBs, finding that essentially all systems form through dynamically stable RLO MT interactions prior to the first SNe (Rappaport & van den Heuvel 1982; Portegies Zwart 1995; Pols et al. 1991). More than half of our Be-XRBs go through a phase of RLO MT initiated at TAMS of the primary followed by MT from a stripped helium companion (Case BB), consistent with previous BPS studies (e.g. Shao & Li 2014; Vinciguerra et al. 2020).

Our rotationally-limited accretion formalism strongly influences the outcome of RLO MT, as stars which accrete only a small fraction of their initial mass are spun up to large fractions of their breakup velocity (Packet 1981). A consequence of this modeling choice manifests in both the implied mass transfer efficiency (β_{rot} , §4.4) which is a focus of many studies in binary stellar evolution (e.g. de Mink et al. 2007), and the ejected circumstellar material from the enhanced wind of the accretor. This ejected circumstellar material can interact with the primary’s subsequent SN, which has been invoked to explain the light curves of hydrogen-poor superluminous supernovae (Stevance & Eldridge 2021), or SNe with multiple peaks in their light curves (Li et al. 2020). Thus, in future studies with POSYDON we may explore the correlation between post-MT binary populations and the occurrence of circumstellar interacting SNe.

Another predicted population formed through MT interactions include stripped helium stars with Be companions (sdO/Be binaries; e.g. Shao & Li 2014, 2021). Although challenging to detect (Ramachandran et al. 2023), observed sdO/Be binaries have been used to derive MT efficiencies, often suggesting highly conservative MT (Schootemeijer et al. 2018; El-Badry et al. 2022). While some of our models undergo nearly conservative MT, they represent a negligible fraction of the total population, which instead evolve through highly non-conservative MT. However, it is challenging to make a direct comparison as not all sdO/Be binaries enter an XRB phase (which we consider in this study), as the left-over He core is not always massive enough to form a CO and remain bound after the SN. Therefore, a dedicated investigation is needed to compare these populations in the future.

5.4. Rotational evolution of Be stars

If, as a large body of evidence suggests (e.g. El-Badry & Quataert 2021; El-Badry et al. 2022; Dodd et al. 2023), the majority of Be stars are the result of binary interactions, then we can gain insights into the Be phe-

nomenon by comparing our results to observations of Be stars at large. Remarkably, our models successfully reproduce multiple features of the observed rotational distribution of Be stars.

The bimodal rotational distribution in Figure 8 is well separated in donor mass, where low mass stars (late-type B) have much higher critical rotation rates than their more massive counterparts (early-type B) which is in agreement with observations of the mean v/v_{crit} increasing for later spectral type stars (Yudin 2001; Cranmer 2005; Balona & Ozuyar 2021). Further, our rotational distribution of donors in Be-XRBs is in excellent agreement with the diversity of rotation rates measured for Be stars ranging from $0.3 < v/v_{\text{crit}} < 0.95$ with a peak measured at $v/v_{\text{crit}} \simeq 0.65 - 0.7$ (Cranmer 2005; Zorec et al. 2016; Balona & Ozuyar 2021).

We expect the morphology of the rotational distribution to change with our assumed binary stellar evolution physics (e.g. Jagadeesh et al. 2023), metallicity (e.g. Liu et al. 2024; Misra et al. 2023), and adopted star formation history, making measurements of Be star rotational distributions in diverse environments of high interest. We leave a thorough parameter study predicting said rotational distributions of Be stars in binaries to future work.

5.5. Donor masses of Be-XRBs

The spectral type distribution of Be stars in star clusters is observed to be bimodal with peaks at early (\sim B0-B2) and late (\sim B5-B8) spectral types (e.g. Mermilliod 1982; Mathew et al. 2008a,b; Yu et al. 2015; Aidelman et al. 2018; Jagadeesh et al. 2023, and references therein). However, late-type Be stars are not present in the Galactic Be-XRB donor population, which is firmly peaked at early spectral types (B0-B2) corresponding to about $M_d \simeq 15 M_{\odot}$ (Fortin et al. 2023). This lack of low mass donors in Be-XRBs is often attributed to the stability and/or efficiency of RLO MT, that preferentially disfavors their formation (Shao & Li 2014; Vinciguerra et al. 2020; Igoshev et al. 2021). Reproducing the mass distribution of Be-XRBs has long been recognized as a challenge for theoretical models (Portegies Zwart 1995), and is often considered an open question in BPS studies.

With our implementation of rotationally-limited accretion in POSYDON, we have shown in Figure 7 our population exhibits highly non-conservative MT, with a RLO MT efficiency distribution peaking around $\bar{\beta}_{\text{rot}} \simeq 5\%$. When comparing to other BPS studies which explore an equivalently low value of the MT efficiency, we produce similar results, finding a donor mass distribution which peaks around $M_d \simeq 3 - 5 M_{\odot}$ (e.g. Shao & Li 2014; Vinciguerra et al. 2020; Igoshev et al. 2021), in tension with

the observed Be-XRB donor mass distribution. One way the aforementioned BPS studies successfully match the observed donor mass distribution is by increasing the MT efficiency of all binary interactions – a modeling choice we cannot trivially adopt in our POSYDON binary MESA models. Thus, our fiducial BPS model is unable to reproduce the observed Be-XRB donor mass distribution. However, we maintain the improved physical accuracy and interpretation of our MT efficiency distribution.

If MT efficiency is well described by our rotationally-limited accretion models, our study suggests another source of preferential selection disfavoring lower mass donors in Be-XRBs. This may be due to selection effects not yet considered from the Be phenomenon including its dependence on spectral type or evolutionary state (e.g. Be vs Bn stars; Mathew et al. 2008a; Cochetti et al. 2020), and measured disk properties (density, duty cycle, and/or emission physics; Vieira et al. 2017).

If, on the other hand, MT efficiency is more conservative than our detailed models suggest, our present study demonstrates the need for new treatment beyond our rotationally-limited accretion formalism, marking a significant step toward a physical interpretation of the MT efficiency in BPS studies. For example, in the future, we may incorporate additional angular momentum loss mechanisms into POSYDON models, such as anisotropic winds due to gravity darkening (Georgy et al. 2011), angular momentum transport from the decretion disk (Krtićka et al. 2011), and/or the winds launched from the disk itself (Ressler 2021).

5.6. On the dearth of BH Be-XRBs

We find a significantly higher frequency of NS Be-XRBs, suggesting BH Be-XRBs are much less likely to be in the intrinsic Galactic Be-XRB population, primarily due to MT interactions and the rarity of BH progenitor stars. This is consistent with observations finding nearly all Be-XRBs with characterized CO companions harbor a NS (Reig 2011), with one tentative BH Be-XRB claimed (MWC-656; Casares et al. 2014, however Janssens et al. 2023 favor a NS or less massive companion).

While it has been shown that the prevalence of NS hosting Be-XRBs is sensitive to the adopted binary stellar evolution physics including RLO MT (e.g. Belczynski & Ziolkowski 2009; Shao & Li 2014), we have demonstrated in Figure 9, the parameterization of the Be phenomenon itself can have a comparably large impact on the ratio of BH to NS Be-XRBs. This suggests that inferences drawn from Be-XRB BPS studies may be obfuscated by the uncertainties underlying the

Be phenomenon, highlighting the importance of theoretically studies reproducing the Be phenomenon self-consistently (e.g. [Ressler 2021](#)), and predicting rotational distributions of Be stars to compare with observations.

Moreover, the number ratio of BH to NS Be-XRBs ([Figure 9](#)) should be considered an upper limit as accretion luminosity selection effects will down-weight BHs compared to NSs in similar accretion conditions ([Brown et al. 2018](#)). Since the number ratio of BH to NS Be-XRBs is a strong function of the threshold rotation chosen for the Be phenomenon, the discovery of BH Be-XRBs may provide valuable constraints on the Be phenomenon itself and binary stellar evolution models.

5.7. Caveats

To compare with the Galactic sample, we adopt models at solar metallicity and use a constant star formation history, although it has been shown the Milky Way has a more complex metallicity distribution and star formation history (e.g., [Snaith et al. 2015](#)). Since this is the first study to explore the self-consistent rotational evolution of Be-XRBs along their HMS-HMS evolution, we use these approximations as these are consistent with previous BPS studies (e.g. [Breivik et al. 2017](#)) and serve as a benchmark for comparison for future studies. Moreover, the complex selection effects in HMXB analyses strongly influence our predicted distribution of Be-XRBs, which may be comparable deviations introduced by changing our fiducial assumptions about the Milky Way.

In our fiducial Be-XRB models, we use a conservative⁴ critical rotation cutoff of $\omega/\omega_{\text{crit}} > 0.5$, where we assume the Be phenomenon is fully efficient while the star is above the threshold. However, it is well known the Be phenomenon is inherently transient, with a duty cycle linked to the hereto unknown disk launching mechanism(s) (e.g. Be vs. Bn stars; [Cochetti et al. 2020](#)), and the structural evolution directly observed in Be star disks ([Vieira et al. 2017](#)). Therefore a complete treatment of Be-XRB observables must include more detailed treatment of disk formation scenarios. However, as we have shown, even with these simplifying assumptions we are able to match a substantial number of observable properties of the Galactic Be-XRB population.

When considering the bimodal rotation distribution explored in [Figure 4](#) and [Figure 8](#), we note that model-

ing the detached phase is performed using pre-computed single-star models which cannot self-consistently evolve the stellar structure in response to rapid rotation. Since rotational effects may significantly alter the evolution of stars rotating close to their critical limit ([Georgy et al. 2011](#)), we expect the peak present in our models at $\omega/\omega_{\text{crit}} \approx 0.99$ to be shifted and or smoothed out to lower values of $\omega/\omega_{\text{crit}}$ which would be further in line with observational studies emphasizing the paucity of near critically rotating Be stars ([Zorec et al. 2016](#); [Balona & Ozuyar 2021](#))

We do not vary uncertain parameters (as is standard in BPS studies) such as the common-envelope efficiency ([Belczynski & Ziolkowski 2009](#)), or SNe models and kick prescriptions ([Igoshev et al. 2021](#)), as we expect these uncertainties to be comparable to those introduced in modeling the Be phenomenon itself and other complex selection effects present for HMXBs. Furthermore, we expect the physical mechanisms forming the rotational distributions highlighted in this study to be robust against such choices.

While POSYDON v1 is unable to model systems which go through a successful CE with two H-rich stars followed by a second phase of MT, [Fragos et al. 2023](#) have shown the fraction of systems evolving through this channel is negligible $\sim 0.3\%$, and thus, do not impact the present study.

6. CONCLUSIONS

We have modeled Be X-ray binaries (Be-XRBs) using the POSYDON binary population synthesis (BPS) code ([Fragos et al. 2023](#)) performing a detailed study of the population-level spin evolution of stars undergoing Roche-lobe overflow (RLO) mass transfer (MT), through their detached XRB phase. We use binary MESA models at solar metallicity combined with a constant star formation history, to compare with properties of Galactic Be-XRBs from a select subset of the catalogue compiled by [Fortin et al. \(2023\)](#). We employ the unique modeling capabilities of POSYDON to investigate the role rotation has as a selection criterion for identifying Be-XRB-like systems from our synthetic models. We find that using rapid rotation ($\omega/\omega_{\text{crit}} > 0.5$) as a selection criterion naturally reproduces many features of the observed Galactic Be-XRB population self-consistently.

Our fiducial BPS models in POSYDON are able to reproduce the broad features of the orbital properties of the observed Galactic Be-XRB population. We reconfirm the standard evolution pathway forming Be-XRBs (stable MT) and strengthen the binary formation scenario for Be stars in general, where we have demonstrated the importance of single star effects (structural changes

⁴ Compared to other BPS studies which use a wide range of reported values that are generally at higher cutoffs of $\omega/\omega_{\text{crit}} > 0.7 - 8$ or greater (e.g. [Shao & Li 2014](#); [Misra et al. 2023](#); [Liu et al. 2024](#)), a result of the confusion within the literature about the true rotation rates of Be stars.

towards TAMS and mass dependent winds) and tidal evolution in forming the rotational distribution during detached evolution.

We find the rotational distribution of our model Be-XRBs is bimodal and is in excellent agreement with the literature reported values of Be stars spinning in the range $0.3 \lesssim v/v_{\text{crit}} \lesssim 0.95$ with a peak around $v/v_{\text{crit}} \simeq 0.65$ (Zorec et al. 2016; Balona & Ozuyar 2021). While non-radial stellar pulsations have been shown to successfully form sustained decretion disks for near critical rotators ($\omega/\omega_{\text{crit}} \gtrsim 0.95$), the impulsive magnetic rotator model may be a dominant formation mechanism for producing the Be phenomenon at this secondary peak at more modest rotation rates $\omega/\omega_{\text{crit}} \simeq 0.6$ and below (Balona & Ozuyar 2021).

With the detailed binary simulations from POSYDON, we calculate a rotationally-limited mass-transfer efficiency, $\bar{\beta}_{\text{rot}}$, and consider the population-level distribution MT efficiencies. Our models suggest the majority of systems evolve through highly non-conservative MT with an equivalent $\bar{\beta}_{\text{rot}} \approx 0.05$. This confirms the picture that a significant fraction of Be-XRBs evolve through a sdO/Be phase before the first SN, and are therefore prime candidates for exhibiting circumstellar interacting SNe.

When considering different features in the rotational distribution of our Be-XRBs, our results suggest that BH Be-XRBs are more likely to contain higher mass donors with moderate rotation rates ($\omega/\omega_{\text{crit}} \simeq 0.6$), and be in relatively wider orbits ($P_{\text{orb}} \simeq 100-1000$ d) with a uniform eccentricity distribution. Furthermore, we find that the parameterization of the Be phenomenon itself (the critical rotation threshold) can impact the resulting Be-XRB population at a level comparable to changing the adopted binary stellar evolution physics (e.g. SN models or the efficiency and stability of RLO MT).

In future studies we will explore the metallicity dependence of the rotational distribution of donors in Be X-ray binaries and its dependence on the star formation history in environments such as the Small Magellanic Cloud. With this study, we are now poised to explore more physically motivated mass-transfer prescriptions for binary evolution, where Be-XRBs may be a key population for constraining the physics of RLO MT in interacting binaries. With the ever increasing complexity of Be-XRB models, we may soon uncover the mecha-

nisms responsible for the Be phenomenon, allowing further investigation into open questions in BPS such as CO formation and SNe physics.

ACKNOWLEDGMENTS

The POSYDON project is supported primarily by two sources: the Swiss National Science Foundation (PI Fragos, project numbers PP00P2_211006 and CRSII5_213497) and the Gordon and Betty Moore Foundation (PI Kalogera, grant award GBMF8477). K.A.R. is supported by the Gordon and Betty Moore Foundation (PI Kalogera, grant award GBMF8477) and the Riedel Family Fellowship. K.A.R. also thanks the LSSTC Data Science Fellowship Program, which is funded by LSSTC, NSF Cybertraining Grant No. 1829740, the Brinson Foundation, and the Moore Foundation; their participation in the program has benefited this work. Z.D. acknowledges support from the CIERA Board of Visitors Research Professorship. S.S.B., T.F., and Z.X. were supported by the project number PP00P2_211006. S.S.B. was also supported by the project number CRSII5_213497. Z.X. acknowledges support from the Chinese Scholarship Council (CSC). K.K. acknowledges support from the Spanish State Research Agency, through the María de Maeztu Program for Centers and Units of Excellence in R&D, No. CEX2020-001058-M. E.Z. acknowledges funding support from the European Research Council (ERC) under the European Union’s Horizon 2020 research and innovation program (Grant agreement No. 772086) as well as from the Hellenic Foundation for Research and Innovation (H.F.R.I.) under the “3rd Call for H.F.R.I. Research Projects to support Post-Doctoral Researchers” (Project No: 7933). This research was supported in part through the computational resources and staff contributions provided for the Quest high performance computing facility at Northwestern University which is jointly supported by the Office of the Provost, the Office for Research, and Northwestern University Information Technology. K.A.R. thanks Tomer Shanar, Yoram Lithwick, and Giles Novak for insightful discussions on interpreting observations and accretion disk physics during.

Software: NumPy (van der Walt et al. 2011), SciPy (Virtanen et al. 2020), matplotlib (Hunter 2007), pandas (McKinney et al. 2010), POSYDON (Fragos et al. 2023)

REFERENCES

- Abdul-Masih, M. 2023, A&A, 669, L11, doi: 10.1051/0004-6361/202245653
- Aidelman, Y., Cidale, L. S., Zorec, J., & Panei, J. A. 2018, A&A, 610, A30, doi: 10.1051/0004-6361/201730995

- Asplund, M., Grevesse, N., Sauval, A. J., & Scott, P. 2009, *ARA&A*, 47, 481, doi: [10.1146/annurev.astro.46.060407.145222](https://doi.org/10.1146/annurev.astro.46.060407.145222)
- Balona, L. A., & Ozuyar, D. 2021, *ApJ*, 921, 5, doi: [10.3847/1538-4357/ac1a77](https://doi.org/10.3847/1538-4357/ac1a77)
- Belczynski, K., & Ziolkowski, J. 2009, *ApJ*, 707, 870, doi: [10.1088/0004-637X/707/2/870](https://doi.org/10.1088/0004-637X/707/2/870)
- Breivik, K., Chatterjee, S., & Larson, S. L. 2017, *ApJL*, 850, L13, doi: [10.3847/2041-8213/aa97d5](https://doi.org/10.3847/2041-8213/aa97d5)
- Brown, R. O., Coe, M. J., Ho, W. C. G., & Okazaki, A. T. 2019, *MNRAS*, 488, 387, doi: [10.1093/mnras/stz1757](https://doi.org/10.1093/mnras/stz1757)
- Brown, R. O., Ho, W. C. G., Coe, M. J., & Okazaki, A. T. 2018, *MNRAS*, 477, 4810, doi: [10.1093/mnras/sty973](https://doi.org/10.1093/mnras/sty973)
- Burkart, J., Quataert, E., Arras, P., & Weinberg, N. N. 2012, *MNRAS*, 421, 983, doi: [10.1111/j.1365-2966.2011.20344.x](https://doi.org/10.1111/j.1365-2966.2011.20344.x)
- Carciofi, A. C., & Bjorkman, J. E. 2006, *ApJ*, 639, 1081, doi: [10.1086/499483](https://doi.org/10.1086/499483)
- Casares, J., Negueruela, I., Ribó, M., et al. 2014, *Nature*, 505, 378, doi: [10.1038/nature12916](https://doi.org/10.1038/nature12916)
- Cochetti, Y. R., Zorec, J., Cidale, L. S., et al. 2020, *A&A*, 634, A18, doi: [10.1051/0004-6361/201936444](https://doi.org/10.1051/0004-6361/201936444)
- Corbet, R. H. D. 1986, *MNRAS*, 220, 1047, doi: [10.1093/mnras/220.4.1047](https://doi.org/10.1093/mnras/220.4.1047)
- Cranmer, S. R. 2005, *ApJ*, 634, 585, doi: [10.1086/491696](https://doi.org/10.1086/491696)
- Cyr, I. H., Jones, C. E., Carciofi, A. C., et al. 2020, *MNRAS*, 497, 3525, doi: [10.1093/mnras/staa2176](https://doi.org/10.1093/mnras/staa2176)
- Cyr, I. H., Jones, C. E., Panoglou, D., Carciofi, A. C., & Okazaki, A. T. 2017, *MNRAS*, 471, 596, doi: [10.1093/mnras/stx1427](https://doi.org/10.1093/mnras/stx1427)
- Dallas, M. M., Oey, M. S., & Castro, N. 2022, *ApJ*, 936, 112, doi: [10.3847/1538-4357/ac8988](https://doi.org/10.3847/1538-4357/ac8988)
- de Mink, S. E., Langer, N., Izzard, R. G., Sana, H., & de Koter, A. 2013, *ApJ*, 764, 166, doi: [10.1088/0004-637X/764/2/166](https://doi.org/10.1088/0004-637X/764/2/166)
- de Mink, S. E., Pols, O. R., & Hilditch, R. W. 2007, *A&A*, 467, 1181, doi: [10.1051/0004-6361:20067007](https://doi.org/10.1051/0004-6361:20067007)
- Dodd, J. M., Oudmaijer, R. D., Radley, I. C., Vioque, M., & Frost, A. J. 2023, *MNRAS*, doi: [10.1093/mnras/stad3105](https://doi.org/10.1093/mnras/stad3105)
- El-Badry, K., & Quataert, E. 2021, *MNRAS*, 502, 3436, doi: [10.1093/mnras/stab285](https://doi.org/10.1093/mnras/stab285)
- El-Badry, K., Conroy, C., Quataert, E., et al. 2022, *MNRAS*, 516, 3602, doi: [10.1093/mnras/stac2422](https://doi.org/10.1093/mnras/stac2422)
- Fortin, F., García, F., Simaz Bunzel, A., & Chaty, S. 2023, *A&A*, 671, A149, doi: [10.1051/0004-6361/202245236](https://doi.org/10.1051/0004-6361/202245236)
- Fragos, T., Andrews, J. J., Bavera, S. S., et al. 2023, *ApJS*, 264, 45, doi: [10.3847/1538-4365/ac90c1](https://doi.org/10.3847/1538-4365/ac90c1)
- Franchini, A., & Martin, R. G. 2019, *ApJL*, 881, L32, doi: [10.3847/2041-8213/ab3920](https://doi.org/10.3847/2041-8213/ab3920)
- . 2021, *ApJL*, 923, L18, doi: [10.3847/2041-8213/ac4029](https://doi.org/10.3847/2041-8213/ac4029)
- Frémat, Y., Zorec, J., Hubert, A. M., & Floquet, M. 2005, *A&A*, 440, 305, doi: [10.1051/0004-6361:20042229](https://doi.org/10.1051/0004-6361:20042229)
- Georgy, C., Meynet, G., & Maeder, A. 2011, *A&A*, 527, A52, doi: [10.1051/0004-6361/200913797](https://doi.org/10.1051/0004-6361/200913797)
- Giacobbo, N., & Mapelli, M. 2019, *MNRAS*, 482, 2234, doi: [10.1093/mnras/sty2848](https://doi.org/10.1093/mnras/sty2848)
- Grudzinska, M., Belczynski, K., Casares, J., et al. 2015, *MNRAS*, 452, 2773, doi: [10.1093/mnras/stv1419](https://doi.org/10.1093/mnras/stv1419)
- Grundstrom, E. D., & Gies, D. R. 2006, *ApJL*, 651, L53, doi: [10.1086/509635](https://doi.org/10.1086/509635)
- Hare, J., Pavlov, G. G., Garmire, G. P., & Kargaltsev, O. 2023, *ApJ*, 958, 5, doi: [10.3847/1538-4357/acfdcf](https://doi.org/10.3847/1538-4357/acfdcf)
- Harmanec, P. 1988, *Bulletin of the Astronomical Institutes of Czechoslovakia*, 39, 329
- Hastings, B., Langer, N., Wang, C., Schootemeijer, A., & Milone, A. P. 2021, *A&A*, 653, A144, doi: [10.1051/0004-6361/202141269](https://doi.org/10.1051/0004-6361/202141269)
- Hobbs, G., Lorimer, D. R., Lyne, A. G., & Kramer, M. 2005, *MNRAS*, 360, 974, doi: [10.1111/j.1365-2966.2005.09087.x](https://doi.org/10.1111/j.1365-2966.2005.09087.x)
- Hunter, J. D. 2007, *Computing in Science Engineering*, 9, 90, doi: [10.1109/MCSE.2007.55](https://doi.org/10.1109/MCSE.2007.55)
- Hurley, J. R., Pols, O. R., & Tout, C. A. 2000, *MNRAS*, 315, 543, doi: [10.1046/j.1365-8711.2000.03426.x](https://doi.org/10.1046/j.1365-8711.2000.03426.x)
- Hurley, J. R., Tout, C. A., & Pols, O. R. 2002, *MNRAS*, 329, 897, doi: [10.1046/j.1365-8711.2002.05038.x](https://doi.org/10.1046/j.1365-8711.2002.05038.x)
- Hut, P. 1981, *A&A*, 99, 126
- Iben, Icko, J. 1991, *ApJS*, 76, 55, doi: [10.1086/191565](https://doi.org/10.1086/191565)
- Igoshev, A. P., Chruslinska, M., Dorozzmai, A., & Toonen, S. 2021, *MNRAS*, 508, 3345, doi: [10.1093/mnras/stab2734](https://doi.org/10.1093/mnras/stab2734)
- Jagadeesh, M. K., Mathew, B., Paul, K. T., et al. 2023, *Research in Astronomy and Astrophysics*, 23, 035002, doi: [10.1088/1674-4527/acaf4](https://doi.org/10.1088/1674-4527/acaf4)
- Janssens, S., Shenar, T., Degenaar, N., et al. 2023, *A&A*, 677, L9, doi: [10.1051/0004-6361/202347318](https://doi.org/10.1051/0004-6361/202347318)
- Kamann, S., Saracino, S., Bastian, N., et al. 2023, *MNRAS*, 518, 1505, doi: [10.1093/mnras/stac3170](https://doi.org/10.1093/mnras/stac3170)
- Klement, R., Carciofi, A. C., Rivinius, T., et al. 2017, *A&A*, 601, A74, doi: [10.1051/0004-6361/201629932](https://doi.org/10.1051/0004-6361/201629932)
- Kriz, S., & Harmanec, P. 1975, *Bulletin of the Astronomical Institutes of Czechoslovakia*, 26, 65
- Kroupa, P. 2001, *MNRAS*, 322, 231, doi: [10.1046/j.1365-8711.2001.04022.x](https://doi.org/10.1046/j.1365-8711.2001.04022.x)
- Krtićka, J., Owocki, S. P., & Meynet, G. 2011, *A&A*, 527, A84, doi: [10.1051/0004-6361/201015951](https://doi.org/10.1051/0004-6361/201015951)
- Langer, N. 1998, *A&A*, 329, 551
- Langer, N., Baade, D., Bodensteiner, J., et al. 2020, *A&A*, 633, A40, doi: [10.1051/0004-6361/201936736](https://doi.org/10.1051/0004-6361/201936736)

- Laycock, S., Zezas, A., Hong, J., Drake, J. J., & Antoniou, V. 2010, *ApJ*, 716, 1217, doi: [10.1088/0004-637X/716/2/1217](https://doi.org/10.1088/0004-637X/716/2/1217)
- Li, L., Wang, S.-Q., Liu, L.-D., et al. 2020, *ApJ*, 891, 98, doi: [10.3847/1538-4357/ab718d](https://doi.org/10.3847/1538-4357/ab718d)
- Liu, B., Sartorio, N. S., Izzard, R. G., & Fialkov, A. 2024, *MNRAS*, 527, 5023, doi: [10.1093/mnras/stad3475](https://doi.org/10.1093/mnras/stad3475)
- Livio, M., & Soker, N. 1988, *ApJ*, 329, 764, doi: [10.1086/166419](https://doi.org/10.1086/166419)
- Martin, R. G., Nixon, C., Armitage, P. J., Lubow, S. H., & Price, D. J. 2014, *ApJL*, 790, L34, doi: [10.1088/2041-8205/790/2/L34](https://doi.org/10.1088/2041-8205/790/2/L34)
- Martin, R. G., Pringle, J. E., Tout, C. A., & Lubow, S. H. 2011, *MNRAS*, 416, 2827, doi: [10.1111/j.1365-2966.2011.19231.x](https://doi.org/10.1111/j.1365-2966.2011.19231.x)
- Mathew, B., Subramaniam, A., & Bhatt, B. C. 2008a, *MNRAS*, 388, 1879, doi: [10.1111/j.1365-2966.2008.13533.x](https://doi.org/10.1111/j.1365-2966.2008.13533.x)
- . 2008b, *MNRAS*, 388, 1879, doi: [10.1111/j.1365-2966.2008.13533.x](https://doi.org/10.1111/j.1365-2966.2008.13533.x)
- McKinney, W., et al. 2010, in *Proceedings of the 9th Python in Science Conference*, Vol. 445, Austin, TX, 51–56
- Mermilliod, J. C. 1982, *A&A*, 109, 48
- Meynet, G., & Maeder, A. 2000, *A&A*, 361, 101, <https://arxiv.org/abs/astro-ph/0006404>
- Misra, D., Kovelakas, K., Fragos, T., et al. 2023, *A&A*, 672, A99, doi: [10.1051/0004-6361/202244929](https://doi.org/10.1051/0004-6361/202244929)
- Negueruela, I., Smith, D. M., Reig, P., Chaty, S., & Torrejón, J. M. 2006, in *ESA Special Publication*, Vol. 604, *The X-ray Universe 2005*, ed. A. Wilson, 165, doi: [10.48550/arXiv.astro-ph/0511088](https://doi.org/10.48550/arXiv.astro-ph/0511088)
- Nixon, C. J., & Pringle, J. E. 2020, *ApJL*, 905, L29, doi: [10.3847/2041-8213/abd17e](https://doi.org/10.3847/2041-8213/abd17e)
- Okazaki, A. T. 1997, *A&A*, 318, 548
- Okazaki, A. T., Bate, M. R., Ogilvie, G. I., & Pringle, J. E. 2002, *MNRAS*, 337, 967, doi: [10.1046/j.1365-8711.2002.05960.x](https://doi.org/10.1046/j.1365-8711.2002.05960.x)
- Okazaki, A. T., Nagataki, S., Naito, T., et al. 2011, *PASJ*, 63, 893, doi: [10.1093/pasj/63.4.893](https://doi.org/10.1093/pasj/63.4.893)
- Oppenheimer, J. R., & Volkoff, G. M. 1939, *Physical Review*, 55, 374, doi: [10.1103/PhysRev.55.374](https://doi.org/10.1103/PhysRev.55.374)
- Packet, W. 1981, *A&A*, 102, 17
- Panoglou, D., Carciofi, A. C., Vieira, R. G., et al. 2016, *MNRAS*, 461, 2616, doi: [10.1093/mnras/stw1508](https://doi.org/10.1093/mnras/stw1508)
- Panoglou, D., Faes, D. M., Carciofi, A. C., et al. 2018, *MNRAS*, 473, 3039, doi: [10.1093/mnras/stx2497](https://doi.org/10.1093/mnras/stx2497)
- Patton, R. A., & Sukhbold, T. 2020, *MNRAS*, 499, 2803, doi: [10.1093/mnras/staa3029](https://doi.org/10.1093/mnras/staa3029)
- Paxton, B., Bildsten, L., Dotter, A., et al. 2011, *ApJS*, 192, 3, doi: [10.1088/0067-0049/192/1/3](https://doi.org/10.1088/0067-0049/192/1/3)
- Paxton, B., Cantiello, M., Arras, P., et al. 2013, *ApJS*, 208, 4, doi: [10.1088/0067-0049/208/1/4](https://doi.org/10.1088/0067-0049/208/1/4)
- Paxton, B., Marchant, P., Schwab, J., et al. 2015, *ApJS*, 220, 15, doi: [10.1088/0067-0049/220/1/15](https://doi.org/10.1088/0067-0049/220/1/15)
- Paxton, B., Schwab, J., Bauer, E. B., et al. 2018, *ApJS*, 234, 34, doi: [10.3847/1538-4365/aaa5a8](https://doi.org/10.3847/1538-4365/aaa5a8)
- Paxton, B., Smolec, R., Schwab, J., et al. 2019, *ApJS*, 243, 10, doi: [10.3847/1538-4365/ab2241](https://doi.org/10.3847/1538-4365/ab2241)
- Podsiadlowski, P., Langer, N., Poelarends, A. J. T., et al. 2004, *ApJ*, 612, 1044, doi: [10.1086/421713](https://doi.org/10.1086/421713)
- Pols, O. R., Cote, J., Waters, L. B. F. M., & Heise, J. 1991, *A&A*, 241, 419
- Portegies Zwart, S. F. 1995, *A&A*, 296, 691
- Raguzova, N. V., & Popov, S. B. 2005, *Astronomical and Astrophysical Transactions*, 24, 151, doi: [10.1080/10556790500497311](https://doi.org/10.1080/10556790500497311)
- Ramachandran, V., Klencki, J., Sander, A. A. C., et al. 2023, *A&A*, 674, L12, doi: [10.1051/0004-6361/202346818](https://doi.org/10.1051/0004-6361/202346818)
- Rappaport, S., & van den Heuvel, E. P. J. 1982, in *Be Stars*, ed. M. Jaschek & H. G. Groth, Vol. 98, 327–344
- Reig, P. 2011, *Ap&SS*, 332, 1, doi: [10.1007/s10509-010-0575-8](https://doi.org/10.1007/s10509-010-0575-8)
- Ressler, S. M. 2021, *MNRAS*, 508, 4887, doi: [10.1093/mnras/stab2880](https://doi.org/10.1093/mnras/stab2880)
- Rivinius, T., Carciofi, A. C., & Martayan, C. 2013, *A&A Rv*, 21, 69, doi: [10.1007/s00159-013-0069-0](https://doi.org/10.1007/s00159-013-0069-0)
- Sana, H., de Koter, A., de Mink, S. E., et al. 2013, *A&A*, 550, A107, doi: [10.1051/0004-6361/201219621](https://doi.org/10.1051/0004-6361/201219621)
- Schootemeijer, A., Götzberg, Y., de Mink, S. E., Gies, D., & Zapartas, E. 2018, *A&A*, 615, A30, doi: [10.1051/0004-6361/201731194](https://doi.org/10.1051/0004-6361/201731194)
- Shao, Y., & Li, X.-D. 2014, *ApJ*, 796, 37, doi: [10.1088/0004-637X/796/1/37](https://doi.org/10.1088/0004-637X/796/1/37)
- . 2021, *ApJ*, 908, 67, doi: [10.3847/1538-4357/abd2b4](https://doi.org/10.3847/1538-4357/abd2b4)
- Snaith, O., Haywood, M., Di Matteo, P., et al. 2015, *A&A*, 578, A87, doi: [10.1051/0004-6361/201424281](https://doi.org/10.1051/0004-6361/201424281)
- Stevance, H. F., & Eldridge, J. J. 2021, *MNRAS*, 504, L51, doi: [10.1093/mnrasl/slab039](https://doi.org/10.1093/mnrasl/slab039)
- Struve, O. 1931, *ApJ*, 73, 94, doi: [10.1086/143298](https://doi.org/10.1086/143298)
- Suffak, M., Jones, C. E., & Carciofi, A. C. 2022, *MNRAS*, 509, 931, doi: [10.1093/mnras/stab3024](https://doi.org/10.1093/mnras/stab3024)
- Townsend, R. H. D., Owocki, S. P., & Howarth, I. D. 2004, *MNRAS*, 350, 189, doi: [10.1111/j.1365-2966.2004.07627.x](https://doi.org/10.1111/j.1365-2966.2004.07627.x)
- van der Walt, S., Colbert, S. C., & Varoquaux, G. 2011, *Computing in Science Engineering*, 13, 22, doi: [10.1109/MCSE.2011.37](https://doi.org/10.1109/MCSE.2011.37)
- Vieira, R. G., Carciofi, A. C., Bjorkman, J. E., et al. 2017, *MNRAS*, 464, 3071, doi: [10.1093/mnras/stw2542](https://doi.org/10.1093/mnras/stw2542)

- Vinciguerra, S., Neijssel, C. J., Vigna-Gómez, A., et al. 2020, MNRAS, 498, 4705, doi: [10.1093/mnras/staa2177](https://doi.org/10.1093/mnras/staa2177)
- Virtanen, P., Gommers, R., Oliphant, T. E., et al. 2020, Nature Methods, 17, 261, doi: [10.1038/s41592-019-0686-2](https://doi.org/10.1038/s41592-019-0686-2)
- Wang, L., Gies, D. R., Peters, G. J., & Han, Z. 2023, AJ, 165, 203, doi: [10.3847/1538-3881/acc6ca](https://doi.org/10.3847/1538-3881/acc6ca)
- Webbink, R. F. 1984, ApJ, 277, 355, doi: [10.1086/161701](https://doi.org/10.1086/161701)
- Xing, Z.-P., & Li, X.-D. 2021, ApJ, 920, 67, doi: [10.3847/1538-4357/ac16e1](https://doi.org/10.3847/1538-4357/ac16e1)
- Yu, P. C., Lin, C. C., Chen, W. P., et al. 2015, AJ, 149, 43, doi: [10.1088/0004-6256/149/2/43](https://doi.org/10.1088/0004-6256/149/2/43)
- Yudin, R. V. 2001, A&A, 368, 912, doi: [10.1051/0004-6361:20000577](https://doi.org/10.1051/0004-6361:20000577)
- Zorec, J., Frémat, Y., Domiciano de Souza, A., et al. 2016, A&A, 595, A132, doi: [10.1051/0004-6361/201628760](https://doi.org/10.1051/0004-6361/201628760)

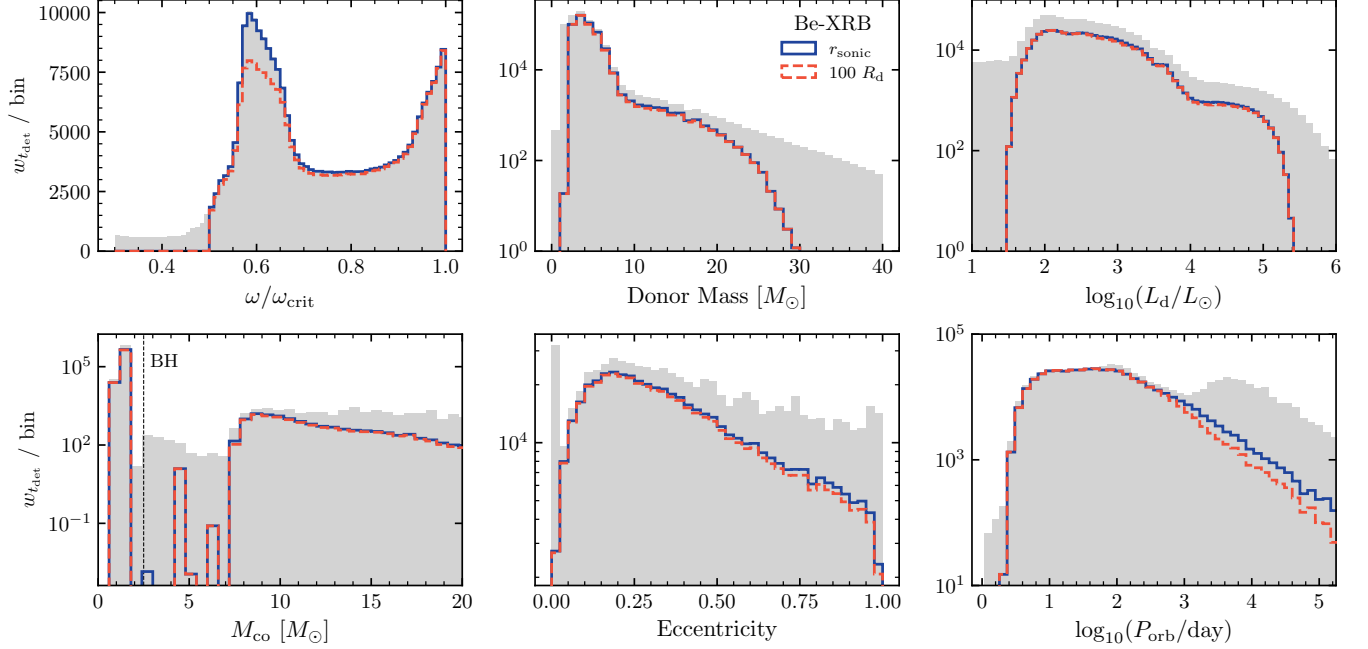


Figure 10. One-dimensional parameter histograms comparing the baseline (gray) and Be-XRB population with two different disk models (§3.3.1), weighted by their detached lifetime ($w_{t_{\text{det}}}$). The interaction criterion compares the decretion disk radius to the periape separation of the binary to determine systems which will produce X-ray emission. The strong overlap in all parameters demonstrates the resulting Be-XRB population is robust to the parameterization of the disk.

Table 1. Formation efficiency of our CO+star baseline population and Be-XRBs organized by mass-transfer evolution during their HMS-HMS phase. The first column indicates the fraction of systems that enter our baseline population out of the initial samples of 2×10^6 binaries, and the fraction of those which eventually become Be-XRBs. The last column indicates the fraction of Be-XRBs that went through a given MT channel.

MT case	Baseline \rightarrow Be-XRB (N)	Be-XRBs (N)	Be-XRBs ($w_{t_{\text{det}}}$)
B	34.0% (56.3%)	33.1%	19.7%
B/C/BB	20.5% (86.9%)	30.8%	47.1%
no RLO	14.7% (2.3%)	0.6%	< 0.1%
A/B	11.9% (44.3%)	9.1%	1.4%
B/C	7.4% (91.5%)	11.7%	14.5%
B/BB	6.4% (94.7%)	10.5%	15.6%
A/B/BB	1.9% (93.5%)	3.1%	1.4%
A	1.7% (14.2%)	0.4%	0.1%
C	1.5% (24.7%)	0.6%	0.2%

APPENDIX

Table 2. Be-XRBs from the catalogue compiled by (Fortin et al. 2023, with references therein), keeping only the systems with Be designations, and measured periods and/or eccentricities.

ID	Spectral Type	P_{orb} [day]	Eccentricity	Used for $e - P_{\text{orb}}$
AX J163904-4642	BIV-V	4.23785	-	False
EXMS B1210-645	B2V	6.7	-	False
4U 2206+543	O9.5Vep	9.558	0.3	True
SAX J0635.2+0533	B2V-B1IIIe	11.2	0.29	True
SAX J2103.5+4545	B0Ve	12.66536	0.4055	True
Cep X-4	B1-B2Ve	20.85	-	False
4U 1901+03	B8-9 IV	22.5827	0.0363	True
1A 1118-615	O9.5III-Ve	24.0	-	False
4U 0115+634	B0.2Ve	24.3174	0.339	True
Swift J0243.6+6124	O9.5V	28.3	0.092	True
H 1553-542	B1-2 V	30.6	-	False
3A 0726-260	O5Ve	34.548	-	False
V 0332+53	O8.5Ve	36.5	0.417	True
XTE J1859+083	B0-2Ve	37.97	0.127	True
KS 1947+300	B0Ve	40.415	0.034	True
H 1417-624	B1e	42.12	0.446	False
AX J1700.2-4220	B0.5IVe	44.03	-	False
RX J2030.5+4751	B0.5V-IIIe	46.02	0.41	False
EXO 2030+375	B0Ve	46.0214	0.419	True
IGR J14488-5942	O-BVe	49.63	-	False
IGR J11435-6109	B0.5Ve	52.46	-	False
AX J1820.5-1434	B0-2 IV-Ve	54.0	-	False
GRO J2058+42	O9.5-B0IV-Ve	55.0	-	False
MWC 656	B1.5-B2IIIe	60.37	0.1	True
4U 1036-56	B0III-Ve	60.9	-	False
RX J0812.4-3114	B0.2IVe	80.39	-	False
HD 119682	B0Ve	90.0	-	False
3A 0656-072	O9.7Ve	101.2	-	False
GS 0834-430	B0-2 III-Ve	105.8	0.14	True
1A 0535+262	O9.5III-Ve	110.3	0.47	True
IGR J19294+1816	B1Ve	117.2	-	False
IGR J11305-6256	B0IIIe	120.83	-	False
GX 304-1	B2Vne	132.5	-	False
SWIFT J1626.6-5156	B0Ve	132.89	0.08	True
RX J0440.9+4431	B0.2Ve	150.0	-	False
SWIFT J1816.7-1613	B0-2e	151.1	-	False
IGR J01363+6610	B1Ve	159.0	-	False
XTE J1946+274	B0-1IV-Ve	172.7	0.246	True
AX J1749.1-2733	B1-3V	185.5	-	False
2E 1145.5-6155	B1III-Ve	187.5	0.5	False
1H 1249-637	B0.5IVpe	226.0	-	False
GRO J1008-57	B0e	247.8	0.68	True
X Per	B1Ve	250.3	0.111	True
SAX J2239.3+6116	B0Ve	262.0	-	False
RX J0146.9+6121	B1IIIe	330.0	-	False
PSR B1259-63	O9.5Ve (γ Be)	1236.724526	0.8698797	True